A DATA DRIVEN MACHINE LEARNING APPROACH TO PREDICTION OF STACKING FAULT ENERGY IN AUSTENITIC STEELS

A Thesis

by

NAYAN CHAUDHARY

Submitted to the Office of Graduate and Professional Studies of
Texas A&M University
in partial fulfillment of the requirements for the degree of

MASTER OF SCIENCE

Chair of Committee,	Raymundo Arróyave
Co-Chair of Committee,	Ibrahim Karaman
Committee Member,	Edward R. Dougherty
Head of Department,	Ibrahim Karaman

August 2016

Major Subject: Materials Science and Engineering

ABSTRACT

The Material Genome Initiative (MGI) calls for establishing frameworks and adopting methodologies to accelerate materials discovery and deployment. The Integrated Computational Materials Engineering (ICME) approach and Materials Informatics leveraging materials data are two very important pillars to the initiative. This research is a data driven materials informatics approach to enable an ICME project on steel alloy design. For the alloy design problem there was a need to predict Stacking Fault Energy (SFE) for any untested alloy composition. SFE is a crucial parameter in determining different deformation regimes in austenitic steels. The SFE itself is dependent on the chemical composition and temperature in steels. There has been considerable study on determination of SFE in steels by experimental and computational methods. While the experimental methods investigate an alloy to find SFE, computational models have been constructed to predict SFE for a given composition and temperature. However, it is shown in this thesis that there are large inconsistencies in experimental data, as well as unavailability of robust computational models to predict SFE in truly multicomponent steel alloys. In this work, a data-driven machine learning approach to mine the literature of SFE in steels with the final aim of predicting deformation regimes for potentially unknown and untested alloy compositions has been demonstrated. Algorithms at the fore-front of Machine Learning have been used to visualize the SFE data and then construct classifiers to predict SFE regime in steels. This machine-learning modeling approach can help accelerate alloy discovery of austenitic steels by linking composition to desired mechanical behavior.

DEDICATION

To Sunita and Pramod Chaudhary,

Because this and everything else in my life is your giving.

ACKNOWLEDGEMENTS

First and foremost I would like to thank my advisor Dr. Raymundo Arroyave from the very bottom of my heart for providing me the opportunity for this particular research. It has affected my life and career in unfathomable ways. More importantly, I thank him for allowing me intellectual freedom and fostering creativity and scientific exploration. Next, I would like to thank all of my lab mates and collaborators who helped me throughout the course of this research. I would especially like to thank Anas Abu-Odeh for his diligent and painstaking help in this research with literature survey and data curation. His contribution is immense and his work is an integral part of this research. I would also like to thank Daniel Sauceda and the MDCS team for helping with the data infrastructure. Lastly, I want to express my gratitude to the one up there, my parents, friends and classmates who kept me going through good and bad times.

NOMENCLATURE

MGI	Materials Genome Initiative
ICME	Integrated Computational Materials Engineering
SFE	Stacking Fault Energy
ML	Machine Learning
TWIP	Twinning Induced Plasticity
TRIP	Transformation Induced Plasticity
FCC	Face Centered Cubic
BCC	Body Centered Cubic
HCP	Hexagonal Close Packed
DFT	Density Functional Theory
GSFE	Generalized Stacking Fault Energy
ANNNI	Axial Next Nearest Neighbor Ising
EMTO	Exact Muffin-Tin Orbitals
CPA	Coherent Potential Approximation
TEM	Transmission Electron Microscopy
WBDF	Weak Beam Dark Field
XRD	X-Ray Diffraction
CALPHAD	Calculation of Phase Diagrams
PCA	Principal Component Analysis
LLE	Locally Linear Embedding
ANN	Artificial Neural Networks
RF	Random Forests
SVM	Support Vector Machines

TABLE OF CONTENTS

Page

LIST OF FIGURES

FIGURE Page

FIGURE Page

LIST OF TABLES

TABLE Page

1. INTRODUCTION

1.1 Thesis Motivation

This thesis is a classic example of "Necessity is the mother of invention". So often in science we start chasing a topic because we dearly need to solve it to help us tackle larger problems. Here I briefly describe the "larger problem" in the context of this thesis. The ultimate objective of this larger problem can be analyzed on two fronts: industry need and scientific merit of approach. The industry need was to design cheaper alloy alternative to existing Ni-based superalloys used for high-temperature applications in advanced ultra supercritical combustion coal-fired power plants. With an aim to increase the cost efficiency of these plants, there was a need to design for higher operating temperatures and pressure. Since the constraint of cost-efficiency was key, stainless steels were identified as the target class of materials. However, to design stainless steels for application at the needed operating environments was a very challenging materials engineering problem. The scientific merit of this project is the design methodology. A traditional experimental approach to designing an alloy for a given application would have made the problem intractable, just by the sheer number of trial and error iterations needed to find the right alloy in such a complex design space. Hence an Intergrated Computational Materials Engineering(ICME) approach was adopted which would significantly reduce the design space by efficient computational search of composition given constraints established by the needs of the material and operating environment.

The computational problem was established to design a class of advanced austenitic stainless steels which would demonstrate ultrahigh strength, ductility, high-temperature strength, creep and corrosion resistance. The strategy to achieve the above objectives

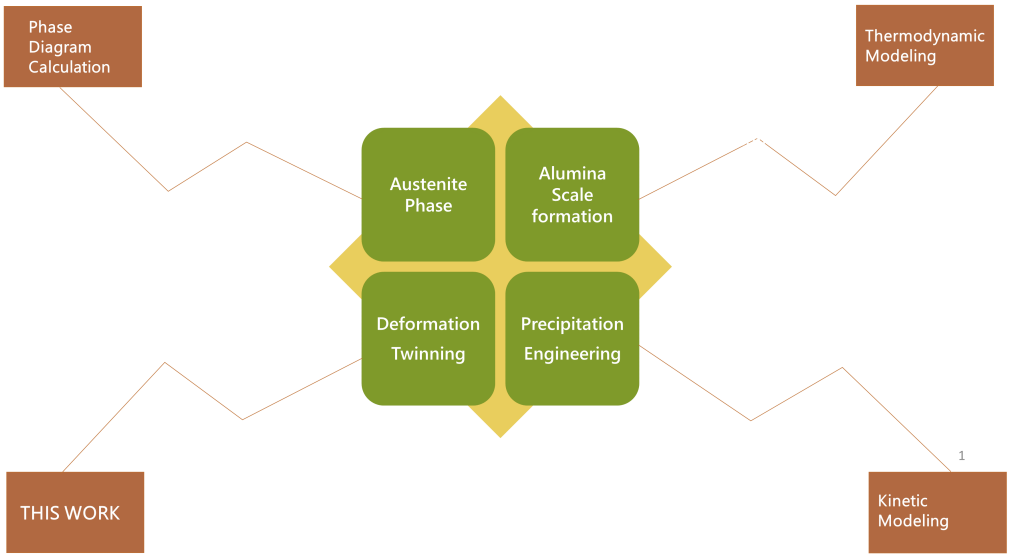

Figure 1.1: Computational design strategy for advanced austenitic stainless steel design

was mapped out as forming alloys with completely austenitic phase, grain-boundary engineering to achieve high density of low energy twin boundaries, precipitation engineering to achieve high temperature intergranular carbides, nitrides for creep resistance and finally alumina surface oxide instead of traditional chromia oxide for enhanced performance in water-vapour environment. A summary of the design strategy and available modeling techniques is shown in Fig. 1.1

As seen in the figure, different modeling techniques either existed or were developed separately for the computational alloy design work. However currently there exists no robust models in the literature to map austenitic steel composition to ease/propensity of twinning or deformation characteristics in general. Hence the sole aim of this work was to develop a predictive model which could do the above and hence aid in selection of compositions for a target deformation in austenitic

steels.

1.2 Stacking Fault Energy and Deformation Regimes

It is well established in literature that the secondary deformation mechanisms in austenitic steels are primarily a function of their SFE in addition to other deformation parameters like strain-rate. Many researchers have calculated different SFE regimes correlated with different deformation behavior. With decreasing SFE, the deformation mechanisms change from (i) dislocation glide to (ii) dislocation glide + mechanical twinning to (iii) dislocation glide + martensitic transformation. Hence being able to compute SFE for any given austenitic steel composition is extremely crucial to steel alloy design since a certain desired mechanical deformation behavior is one of the most important design criteria. Unfortunately, currently there doesn't exist a robust go-to equation in the literature that the authors know of which can be used to compute the SFE or predict possible deformation behavior of an untested austenitic steel composition.

1.3 MGI and Materials Informatics

The Materials Genome Initiative (MGI) [26] emphasizes on using new frameworks and techniques to accelerate materials discovery. One of the pillars and new paradigms of this initiative leading to rapid materials discovery is Materials Informatics [72] and Materials Data Science [32]. Materials Data science and informatics encapsulates Machine Learning/Statistical Learning/Data Mining or various other interchangeably used terminologies which are being used in myriad disciplines ranging from product-based fields like artificial intelligence, social media analytics, decision making in enterprises to economics, bioinformatics, astronomy and other scientific fields. The sole basis of these learning algorithms is that given some information or data and an understanding of what that data means, an underlying pattern

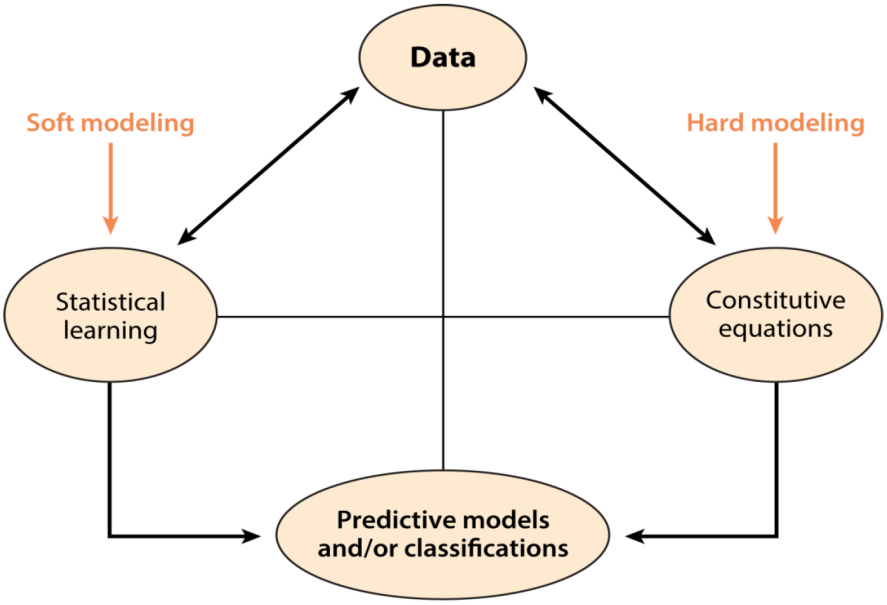

Figure 1.2: Two competing approaches to predictive modeling of material properties [72]

can be uncovered and 'learnt' which can be used to predict outcomes for unseen scenarios. These powerful algorithms have immensely contributed to development and success of the above discussed disciplines, specifically where the complexity of the problems rendered theoretical modeling based on domain knowledge incredibly challenging. Materials Informatics is the paradigm which leverages these techniques on top of the experimental and physics-based computational data in materials sciences community to usher the field forward in a new era of accelerated materials discovery.

1.4 This Work

Having provided the motivation and established the problem statement, a brief summary of this thesis objective is provided below. As described above, for austenitic steel design with a certain desired mechanical deformation behavior, SFE is the crucial parameter. SFE itself is a predominantly a function of temperature and composition. Therefore to design multicomponent austenitic steel, there needs to be a model connecting composition and SFE. However as explained, there isn't one currently. In absence of a robust physics based model, we leverage machine learning models to predict SFE regimes based off all the experimental data on calculation of SFE for different austenitic steel compositions. Hence what we are doing is trying to build a lower, workable representation of the composition-SFE relationship relying on soft, statistical modeling because the true, higher representation is too expensive to model or unrealistic to work out with the current knowledge.

Although the project motivation was to build a predictive model to predict ease/propensity for twinning given austenitic steel composition, this work goes beyond that. It addresses the key problem of relating composition to SFE in austenitic steels, albeit in a practical, inexpensive way that will enable alloy design. The other merit of this work is that it is an apt showcase of the Materials Informatics approach. A complete workflow is developed: (i) Collecting and curating materials data (ii) Using machine learning/ statistical modeling to mine the data (iii) Extract knowledge from the data mining task

2. LITERATURE SURVEY

In this section we very briefly discuss the origin of stacking faults and SFE in steels. Then a thorough description of the existing modeling techniques for SFE prediction and their pitfalls have been discussed. Finally an exhaustive study of all experimental research in SFE calculation of austenitic steels has been presented. As pointed out earlier, there are large inconsistencies in the experimental SFE data. In the study of experimental research, this aspect of SFE data is also discussed. The inconsistencies provide a major impediment to SFE modeling and hence one of the crucial merits of the approach in this work is handling these inconsistencies.

2.1 Stacking Fault Energy

Austenitic steels are steels with complete austenite phase at room temperature. Since austenite is the face-centered cubic (fcc) allotrope of Fe, austenitic steels have fcc structure at room temperature. In fcc structure, the close-packed {111} planes are stacked in an ABCABCABC... sequence. Slip in fcc systems occurs on the {111} planes in <110>direction. When a dislocation slips in this direction, it leaves behind a perfect lattice in the same sequence and hence called perfect dislocations. However it is sometimes more energetically favorable for the perfect dislocations to dissociate into *Shockley partials* wherein the dislocation direction now changes to <112>and these dissociated dislocations are called partial dislocations. These partial dislocations change the local stacking of the crystal from ABCABCABC... to ABC<u>AC</u>ABC.. This local change in stacking is called a stacking fault and the local stacking is changed as if it is hcp ABABAB... This stacking fault is specifically called an intrinsic stacking fault where the fault occurs as if one plane(B) was removed. There is another kind of stacking fault called the extrinsic stacking fault where the

stacking changes from ABCABCABC.. to ABCACBCABC... This is as if an extra plane(C) was added. However intrinsic faults are easier to form and most properties depend on them. The discussion in this thesis has been hence limited to intrinsic stacking faults and energy primarily. Now the width of the formed stacking fault is dependent on the stacking fault energy. Higher stacking fault energy leads to relatively narrower stacking faults and vice versa. Stacking fault energy primarily depends on the composition of the material and temperature. Other effects like grain size and processing are disputed to have effects[96, 19] however evidence is minimal or the effects are insignificant and hence the discussion is limited to composition and temperature.

2.1.1 Stacking Fault Energy and Deformation Mechanisms

The secondary deformation mechanisms in steels is primarily dependent on SFE. There has been previous work in this direction by many researchers which establishes that deformation mechanisms in Austenitic Steels are a function of SFE 'regimes'. Fig. 2.1 shows different SFE regimes proposed in literature. Although the research establishes different values for these regimes, they are close and there is a common acceptance in literature. It is well accepted that an austenitic steel with SFE value below 20 mJ/m^2 deforms by martensitic transformation of TRIP-like behavior, with SFE value in between 20 mJ/m^2 and 45 mJ/m^2 deforms primarily by deformation twinning leading to a TWIP-like behavior while SFE values above 45 mJ/m^2 deforms majorly by slip. These regimes can be called Low, Medium and High respectively. What also helps is that this mapping from SFE regime to deformation mechanism is monotonic as well as one-to-one.

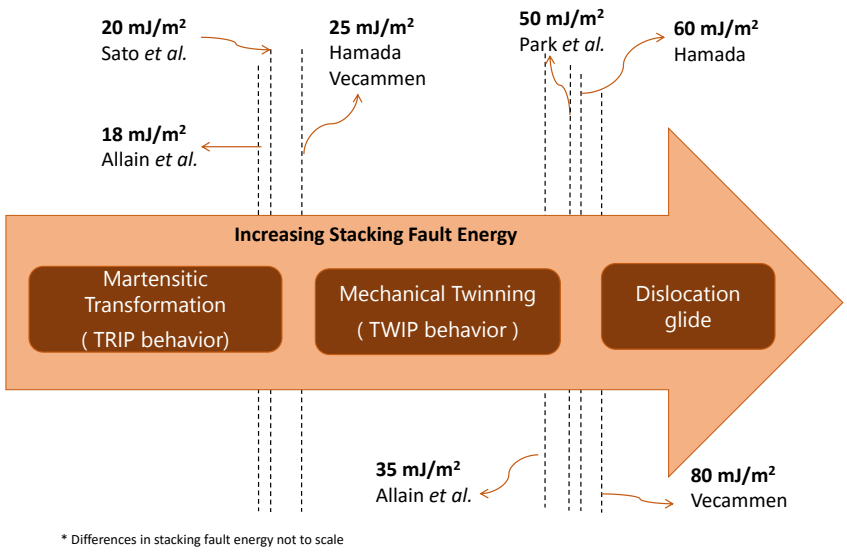

Figure 2.1: Different boundary values in literature for SFE regimes

2.2 Theoretical Prediction of Stacking Fault Energy

There have been predominantly three approaches to predicting stacking fault energy for any given composition in austenitic steels. (i) First Principles/Ab-initio Electronic Structure calculations, (ii) Thermodynamic Modeling and (iii) Linear Regression. While the first two are physics based modeling paradigms, the latter is a purely statistical approach. The modeling techniques and their issues are very briefly discussed below.

2.2.1 Physics Based Modeling

There is substantial work in the literature where material science fundamentals have been used to predict SFE for alloy compositions. One very important formulation is the thermodynamics or CALPHAD approach where the energy of the stacking

fault is modeled as a martensitic embryo or a hcp second phase with phase boundaries lining the austenite or fcc phase on either sides. Another significant approach is using first principles, ab-initio electronic structure modeling based on quantum mechanical theory. Within first principles, the SFE is modeled using different approaches which will be discussed briefly ahead.

2.2.1.1 First Principles Calculations

Calculation of SFE in steel alloy system by first principles, ab-initio electronic structure modeling based on quantum mechanical theory can be realized by more than one approach. However the choice of approach is eventually guided by computational cost and accuracy of method. Though these methods are essentially predicting a composition-SFE relationship, there aren't as many investigations as the limitation is relatively straight-forward. With current computational resources it is almost impossible to do first-principle calculations of SFE for multi-component steels with many alloying additions which is a practical need in alloy design. In fact the most complex chemistry for which the SFE has been modeled and predicted using ab-initio approaches are quaternary steel alloys.[88, 53]

There are predominantly two approaches in the literature for calculating SFE of Fe alloyed with other elements. One approach was first presented by Vitos and co-authors[88] who calculated the intrinsic SFE in ternary and quaternary Fe alloys by adopting a Axial Next Nearest Neighbor Interaction (ANNNI) model for ferrous alloys. Another approach is the widely known calculation of Generalized Stacking Fault Energy(GSFE) surface which claims to provide a complete description of the stacking fault energy. Based on accuracy and computational cost, the approach from Vitos seems to be the better atleast for the ferrous alloys or steel alloy system. A high-level description of both approaches is explained next.

The approach pioneered by Vitos is the ANNNI model which is an extension of the ideas used to calculate SFE and explain interlayer interactions in SiC polytypes. [11, 15]. For SiC these authors adopted the original Axial Next Nearest Neighbor Ising model by replacing the Ising spin with interaction between layers, and hence the name of Axial Next Nearest Neighbor Interaction model. In their paper[88], Vitos formulates the formation energy of an intrinsic stacking fault in a fcc crystal as the excess free energy per unit area:

$$\gamma = \frac{F_{SF} - F_0}{A_{2D}} \tag{2.1}$$

F_{SF} is the free energy of the system with the stacking fault, F_0 is the free energy of system without stacking fault and A_{2D} is the area of the stacking fault. With the ANNNI model, the stacking sequence along a direction is represnted by S_i's, the same formulation as Ising model but here they represent different layers rather than spins. The excess free energy of a stacking sequence is then formulated in terms of $-\Sigma_i \Sigma_j J_n S_i S_{i+n}$ where J_i is the interaction parameter for the i^{th} nearest neighbor. Hence J_1 is nearest neighbor, J_2 is the next nearest neighbor and so on and so forth. Using this representation, the energy of intrinsic SFE can be expressed and also for periodic structures like fcc, hcp and dhcp. Based on these expressions:

$$F_{SF} - F_0 \approx F_{hcp} + 2F_{dhcp} - F_{fcc} \tag{2.2}$$

Here the reason for approximate symbol is since the expressions in terms of J_i are truncated and only the first three or four interactions are taken. Although these approximations have shown to be consistent and within the limits of experimental error, for higher precision higher order terms need to be considered. The calculations were then done based on the EMTO-CPA approach also devised by the same author.

For a detailed description one can refer to their work.[88]

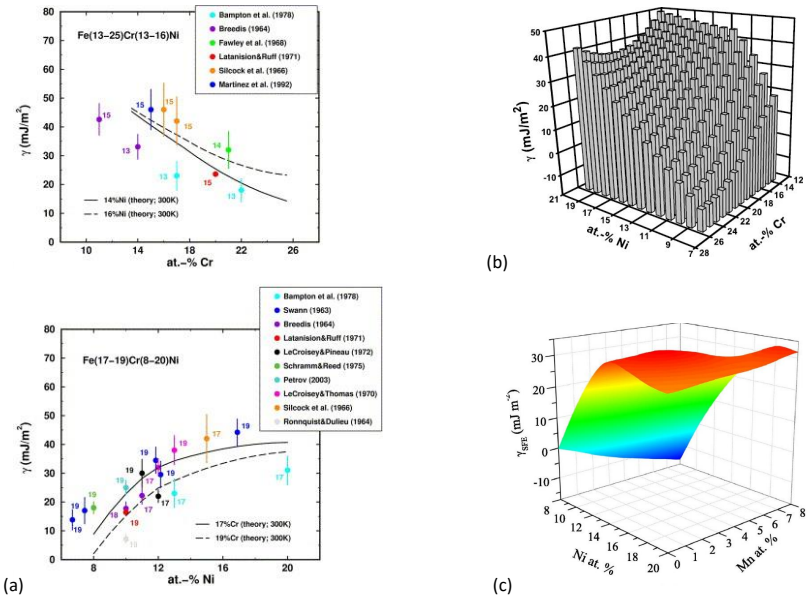

Figure 2.2: a) Comparison of theoretical calculations of SFE by ANNNI model with experimental values[88] b) Non-linear dependence of SFE on composition of Ni and Cr [87] c) Non-linear dependence of SFE on composition of Mn based on host composition of Fe-Cr-Ni [53]

The authors have modeled ternaries like Fe-Cr-Ni[88, 87, 53] systems as well as quaternaries like Fe-Cr-Ni-Mn[88, 53], Fe-Cr-Ni-Nb[88, 53] and Fe-Cr-Ni-Co[88, 53]. These results have been shown to be good agreement with the experimental values keeping in the mind the inconsistencies and uncertainty of experiments. Fig2.2a shows the comparison. The formulation has also and excellent description for the temperature variance of SFE which has been modeled by magnetic contributions. The biggest contribution of the above approach and research has been to explain the nature of composition-SFE relationship. The authors have modeled over a range

of compositions for the ternaries and quaternaries and have found highly non-linear relationships[88, 87, 53]. They have shown that the effect of an alloying element on SFE depends not only the element but also on the host composition, i.e the values of other elements. Fig2.2b and Fig2.2c demonstrate these non-linear relationships. Thus the authors have claimed that it is impossible to derive universal SFE-composition relationships for multi-component steel alloys.

The other approach is the widely used and known technique for calculating SFE in elemental metals and alloys called the Generalized Stacking Fault Energy calculation which is a comprehensive definition of the stacking fault energy. In fcc system, a single-layer of stacking fault can be generated by displacing the upper half of the crystal relative to the lower half along <112>direction on the {111} planes. The fault energy γ can be calculated as a function of this displacement, which will be a curve representing energy of different sheared configurations resulting from different values of displacement along <112>. There are some important characteristic material properties which can be calculated based on the GSFE curve which have been depicted in Fig.2.3. There are three main quantities i.e. the unstable fault energy, intrinsic fault energy and stable fault energy. The displacements which lead to the structures corresponding to these energies are $0.5|b_p|$, $|b_p|$ and $2|b_p|$ respectively where $|b_p| = 1/6$<112> is the Burger's vector of the partial dislocation producing the shear.

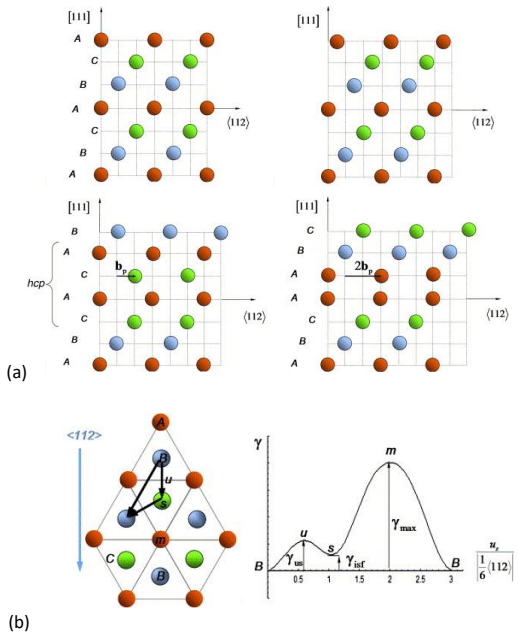

Figure 2.3: a) A representation of different shear displacements to calculate GSFE curve b) Schematic of a calculated GSFE curve with important quantities indicated[34]

However the use of this approach has not yielded good quantitative results of SFE in the Fe alloy system. The calculations using this approach for Fe alloy system were first performed by Kibey and co-authors [34]. The authors modeled the Fe-N binary and Fe-Mn-N ternary systems. The same approach has been adopted in literature to model other alloying additions in iron system like Fe-Mn binary[16], Fe-C binary[1], Fe-Cr-Ni ternary[52] , Fe-Mn-Al-C quaternary[55] and Fe-X binaries where X=transition metals[51]. As mentioned earlier, the important note about all these calculations is that they all severely underestimate intrinsic SFE compared to similar experimental and theoretical (thermodynamic and other ab-initio approaches) data, even taking into account that these are 0 K calculations. Hence most of these GSFE calculations are restricted to explaining trends of SFE variation in particular alloy

system.

In summary ab-initio electronic structure modeling is a fundamentally robust approach to predicting SFE in steel alloys, specifically the ANNNI model has been shown to have excellent agreement with experimental values. However due to computational cost and complexity, these calculations are impossible for multi-component alloys with many alloying additions. They however provide crucial insights about the nature of the composition-SFE relationship in the steel alloy system.

2.2.1.2 Thermodynamic Modeling

There have been many investigations into calculation of SFE using the thermodynamics or CALPHAD approach where the energy of the stacking fault is modeled as a martensitic embryo or a hcp second phase with phase boundaries lining the austenite or fcc phase on either sides. The schematic of such a formulation has been shown in Fig. 2.4. As shown the SFE can then be written out in terms of extra energy needed to nucleate this stacking fault, which is the Gibbs Free energy to to nucleate the locally hcp stacking fault i.e. $\Delta G_{fcc \rightarrow hcp}$, the strain energy due to the stacking fault as a second phase in the fcc matrix and partial dislocations bounding the stacking fault i.e. E_m^{str} and the interfacial energy on the hcp-fcc boundary i.e. σ.

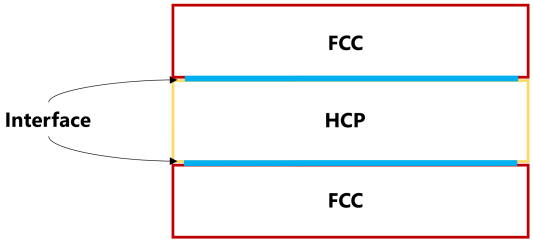

$$\gamma_{SFE} = 2\rho\left(\Delta G_m^{\gamma\rightarrow\varepsilon} + E_m^{str}\right) + 2\sigma$$

Figure 2.4: Schematic of thermodynamic formulation for SFE calculation

The Gibbs Free energy can be written out as a summation of ideal, excess, magnetic and other sources energetic considerations. Different researchers have modeled various different Fe based systems using slightly varying formulations. For eg. the stacking fault modeled as a hcp second phase can lead to different strain energies based on the shape assumed for the stacking Fault. Olson [64] and Cotes [12] have modeled the second phase as a spherical particle while Ferreira and Mullner [59] model it as flattened plate-like particle. These lead to different strain energy contributions although the energy value itself as well as the differences are low compared to SFE values. However the biggest discrepancy in thermodynamic SFE modeling is in the value of interfacial energy σ. In all research papers this is not physically estimated, neither is there robust experimental data for it. Hence it is generally used as a fitting parameter to make the thermodynamic calculation match experimental SFE calculations. This leads to large discrepancies as the value of σ in literature varies from 4-20 mJ/m^2 [58, 95, 61, 31, 56, 3, 93, 66, 13, 18, 12, 64, 76] which leads to even larger variations in SFE, thus highly depreciating the reliability of the ther-

modynamic models and SFE prediction. Fig. 2.5 demonstrates such an example. In their paper, Akbari and researchers [76] calculate SFE for Fe-Mn-C and other systems. They construct composition-SFE maps choosing different values of σ given in literature since there is no way to determine this as discussed earlier. We consider 2 random compositions on this map and show how the choice of different interfacial energy values leads to a large range of possible SFE for a fixed composition.

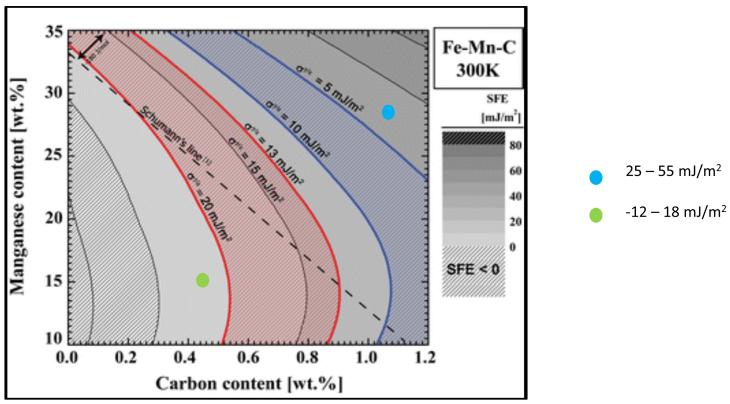

Figure 2.5: An example of variation in SFE due to large uncertainty in interfacial energy parameter [76]

Hence the compositions corresponding to the blue point and green point on the composition-SFE map can have SFE values differing by 30 mJ/m^2 depending on what the interfacial energy parameter is chosen, and this is very unreliable prediction for the purposes of alloy design. Many different papers show many other values of interfacial energy. Also it has been discussed in literature how this value itself is composition dependent and hence estimating it for one composition based on experimental value and then using the same for all other compositions is not physical.

This energy parameter than becomes essentially a fitting parameter that absorbs all unexplained physics in one's model.

To summarize, thermodynamics approach in theory is a good approach for multi-component steels. However the problems lies with databases and energy parameters. Modeling the Gibbs Free energy of fcc to hcp transition needs data for hcp state in the databases for Fe alloys which is lacking. The other significant problem is the interfacial energy parameters which are basically used as fitting parameters in the model leading to high uncertainties and inconsistencies among models in the literature. Sometimes the difference in interfacial energy parameters is so much so that the difference in SFE more or less means an altogether different SFE regime for the same composition. Hence the thermodynamic modeling approach is not as robust as one would need for practical applications.

2.2.2 Statistical Modeling

In addition to the theoretical computational formulations for describing SFE-composition relationship, statistical technique of linear regression has been applied on many small sets of experimental SFE data to describe a linear relationship between SFE and composition. Linear Regression is although much more powerful than just modeling straight lines, none of the papers have tried to model non-linear relationships. Table.2.1 has a list of all such linear regression equations in the literature, which have been formulated for different composition regimes in the austenitic steel system. Most of these equations have been modeled based on the experiments carried out in one research paper which is typically very less. Except for a couple of papers which have either many experiments or took data from other papers, these equations are very "local" in the composition space.

Reference	Technique	Year	Regression Equation	Notes
Schramm *et al. [78]*	TEM	1975	$\gamma = 4{+}1.8\,(\%Ni){-}0.2\,(\%Cr){+}410\,(\%C)$	C: 0.012 to 0.027 %
Schramm *et al. [78]*	TEM	1975	$\gamma = 34 + 1.4\,(\%Ni) - 1.1\,(\%Cr) - 77\,(\%N)$	N: 0.004 to 0.044 %
Schramm *et al. [78]*	TEM	1975	$\gamma = 34 + 2.2\,(\%Ni) - 1.1\,(\%Cr) - 13\,(\%Si)$	Si: 0.01 to 0.59 %
Schramm *et al. [78]*	TEM	1975	$\gamma = 32 + 2.4\,(\%Ni) - 1.2\,(\%Cr) - 1.2\,(\%Mn)$	Mn: 0.001 to 1.56 %
Schramm *et al. [78]*	TEM and XRD	1975	$\gamma = -53 + 6.2\,(\%Ni) + 0.7\,(\%Cr) + 3.2\,(\%Mn) + 9.3\,(\%Mo)$	Excluding minor elements
Rhodes *et al. [75]*	TEM	1977	$\gamma = 17 + 2.29\,(\%Ni) - 0.9\,(\%Cr)$	Fe-Cr-Ni ternary, Low Cr (<20% Cr)
Rhodes *et al. [75]*	TEM	1977	$\gamma = -26.6 + 0.73\,(\%Ni) + 2.26\,(\%Cr)$	Fe-Cr-Ni ternary, High Cr (>20% Cr)
Rhodes *et al. [75]*	TEM	1977	$\gamma = 1.2 + 1.4\,(\%Ni) + 0.6\,(\%Cr) + 17.7\,(\%Mn) - 44.7\,(\%Si)$	Commerical Austenitic alloys
Brofman *et al. [10]*	TEM	1978	$\gamma = 16.7 + 2.1\,(\%Ni) - 0.9\,(\%Cr) + 26\,(\%C)$	5-20% Ni, 9-20% Cr
Yang *et al. [94]*	XRD	1982	$\gamma = -1 + 2.02\,(\%Ni) + 321\,(\%C)$	∼18% Cr
Li *et al. [48]*	TEM	2000	$\gamma = 28.87 + 1.64\,(\%Ni) - 1.1\,(\%Cr) + 0.21\,(\%Mn) - 4.45\,(\%Si)$	5-8% Ni, 7-10% Cr
Tian *et al. [85]*	XRD	2009	$\gamma = 17.53 - 1.30\,(\%Si)$	Fe-31Mn-(0.25-8.67)Si-0.77C (at%)
Ojima *et al. [63]*	TEM	2009	$\gamma = 5.53 + 1.4\,(\%Ni) - 0.16\,(\%Cr) + 17\,(\%N)$	10-25% Cr, 4-25% Ni
Lee *et al. [45]*	XRD	2012	$\gamma = -5.79 + 39.94\,(\%C + N) + 3.81\,(\%C/N)$	Fe-18Cr-10Mn alloys
Jeong *et al. [28]*	Neutron Diffraction	2012	$\gamma = 19 + 8.84\,(\%Al)$	Fe-18Mn-xAl-0.6C alloys
Yonezawa *et al. [96]*	TEM	2013	$\gamma = -7.1 + 2.8\,(\%Ni) + 0.49\,(\%Cr) + 2.0\,(\%Mo) - 2.0\,(\%Si) + 0.75\,(\%Mn) - 5.7\,(\%C) - 24\,(\%N)$	Water cooled samples
Yonezawa *et al. [96]*	TEM	2013	$\gamma = -4.8 + 2.8\,(\%Ni) + 0.44\,(\%Cr) + 2.0\,(\%Mo) - 2.0\,(\%Si) + 0.75\,(\%Mn) - 2.1\,(\%C) - 17\,(\%N)$	furnace cooled samples
Yonezawa *et al. [96]*	TEM	2013	$\gamma = -4 + 2.8\,(\%Ni) + 0.39\,(\%Cr) + 2.2\,(\%Mo) - 2.0\,(\%Si) + 0.75\,(\%Mn) - 0.47\,(\%C) - 12\,(\%N)$	furnace cooled and aged
Lehnhoff *et al. [47]*	TEM	2014	$\gamma = k - 2.6\,(\%Si) + 4.9\,(\%Al)$	Fe-15Ni-11Cr-1Mn alloys
Pierce *et al. [69]*	TEM	2014	$\gamma = -133.4 + 6.26\,(\%Mn)$	Fe-xMn-2.7Al-2.9Si, 25<Mn<27.5%
Pierce *et al. [69]*	TEM	2014	$\gamma = 779.3 - 67.4\,(\%Mn) + 1.496\left(\%Mn^2\right)$	Fe-xMn-2.7Al-2.9Si, 22<Mn<25%

Table 2.1: Linear regression equations for SFE-composition relationship

There are two major problems with the Linear Regression approaches in the literature. First the amount of data used to create these regression models are woefully small. In most cases the models have been built from the few experi-

mental values in the paper, and hence cannot be extrapolated with any degree of certainty. More importantly there has been ample discussion in the literature about the composition-SFE relationship being non-linear and also the significant interaction between amount of elements in alloy to affect the SFE. Hence there cannot be universal regression equations as the effect of one element on SFE depends on the values of other elements in the alloy system. When looking at all the above equations, it is evident that all of them have linear relationships in composition-SFE which is not the true case. These equations are essentially modeled in sections of the whole composition-SFE space, keeping values of some elements constant.For eg, the effect of Ni wt% on SFE is very different in all these equations and also SFE is linearly related to SFE in all cases. As such all these equations cannot be considered as universal compostion-SFE relationships. In order to do robust statistical modeling, a much larger dataset is needed. Also the model should try to mimic the true relationship, hence there is a need to consider non-linear higher order and interaction terms.

2.3 Experimental Calculations of Stacking Fault Energy

Above we discuss the methods for prediction of SFE for untested Fe alloys. However these predictions have to matched against some true value to gauge their accuracy. The true value of SFE is measured by experimental techniques for certain alloy compositions and then the computational theories leverage these for parameter fitting or accuracy purposes. Typically it is difficult to compare values from computational models to experimental observations due to some missing physics in the models, sample preparation inconsistencies, experimental error and other reasons. However the task becomes exponentially difficult when the experimental observations themselves are very uncertain and inconsistent, not only due to experimental error but

the inherent technique of observation or calculation. This the biggest problem with the SFE literature on austenitic steels.

SFE is an intrinsic material property depending on composition and temperature. Although there have been a very few papers claiming grain size and processing effects, the evidence is minimal or the effects are small which can be ignored. Despite being a material property, there is no direct way to measure SFE. For example, the strength of a material can directly be determined by a tensile test. There can be uncertainty in the strength due to experimental error but not due to the method of measurement itself. However in case of SFE, the value calculated is indirect. An observable quantity of the material is theoretically related to the SFE of the material. In this calculation there is then substitution of material constants, the observed property and other material parameters. Hence there are multiple sources of uncertainty and inconsistency. In general there can be error due to observed quantity not matching the exact theoretical requirement to be used to calculate SFE, using averaged value of material properties for multiple compositions, experimental error in the observed quantity and finally the robustness of the underlying theory itself relating and observed quantity to the SFE of material. This all leads to a very complex set of results for SFE of austenitic steels making it very difficult to use for comparisons and trends as well as matching against experimental predictions. Different techniques lead to very different calculations of SFE for similar compositions.

We discuss the two major techniques and methods within them to experimentally measure SFE in austenitic steels. The understanding of this is important as for our modeling we eventually use all the experimental data available to do informatics.

2.3.1 Transmission Electron Microscopy

The oldest and the first used technique for indirectly measuring SFE was using transmission electron microscopy(TEM). Although this is referred to as the direct method sometimes, it is essentially indirect as it related geometry of dislocations and other defects to the SFE of the material. Many different geometries were earlier related to SFE like extended dislocation nodes, extrinsic-intrinsic stacking fault pairs, stacking fault tetrahedra and most recently partial dislocation separation. Over the years extended dislocation nodes became the method of choice and currently due to availability of better instrumentation and hence resolution, partial dislocation separation is the most commonly used method. Theoretically it is the most simple as the separation between the partial dislocations is the width of stacking fault itself which can be directly related to energy. All other methods are geometrical workarounds for calculating SFE. Fig. 2.6 shows the 2 most commonly imaged geometries from a certain composition of steel.

Though the TEM technique is theoretically most reliable experimental method, specially the partial dislocation separation, the problems arise due to experimental measurement. For high SFE compositions, the partial dislocations are so close that their separation distance calculation can have significant % error with only slight changes in absolute measurement. Moreover one very seldom finds partial dislocation parallel to each other, in reality there is curvature and kinks in the partial dislocation arrangement. Thus the measurement of distance becomes confusing. The extended dislocation node radii measurements have problems with the actual geometry not allowing for proper radii measurements as circles cannot be exactly drawn. Added to all this is the statistical scatter. Since with TEM imaging one can only image a few regions and a few geometries, there is always a question of sample representation by

these few observations. Microstructural effects and interstitials also affect dislocation geometries and hence another criticism is that the geometries are not at equilibrium. Given that SFE depends on temperature and TEM imaging leads to sample heating, there is also scope of measuring SFE at temperatures higher then intended. Some of the above listed error sources are quantifiable while others aren't. Although some papers report the quantifiable experimental error, many don't. Thus all reported values have inherently large scatter that one should be very conscious of before attempting to use the values.

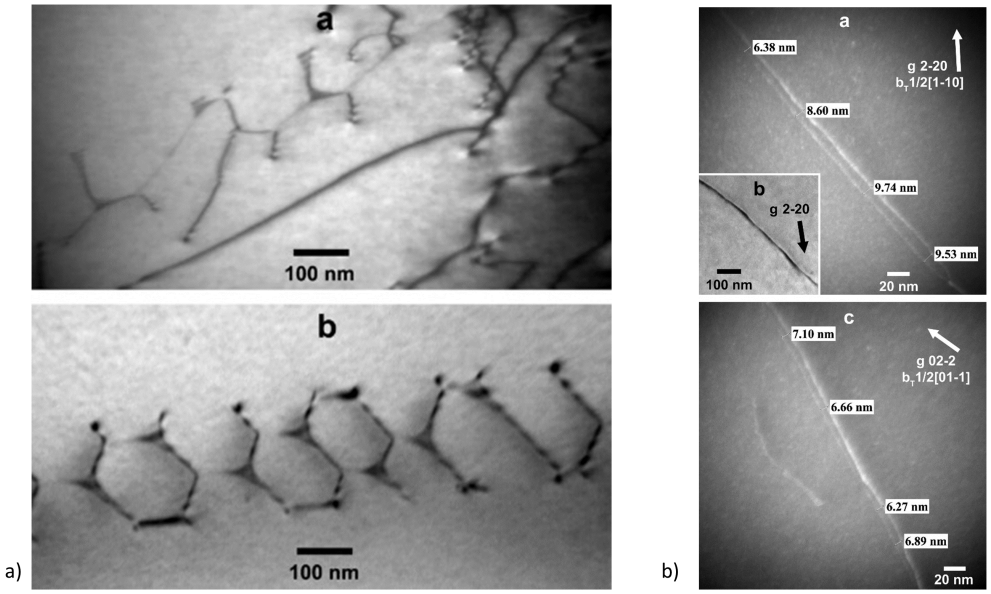

Figure 2.6: Example geometries of dislocations used to measure SFE experimentally using TEM a)Extended dislocation nodes b)Partial dislocation separation [68]

2.3.2 X-Ray Diffraction

TEM is a widely used and established direct method for experimental determination of SFEs. However it is a tedious method, strictly for low SFE materials where dislocation pairs can be adequately resolved and with questionable statistical significance due to very small percentage imaging volume of the total sample volume. Consequently indirect methods were suggested but the research from Reed and Schramm [73] is the seminal work in using X Ray diffraction technique for calculation of SFEs. The authors established a relationship between SFE, stacking fault probability and rms microstrain which made it possible to calculate SFE rather than just reporting stacking fault probability as was done earlier. Based on the above formulation, Schraam and Reed published the first work for calculation of SFE using X Ray diffraction in commercial austenitic steels [78] and Fe-Ni alloys [79]. The equation formulated by the authors is [73]:

$$\gamma = \frac{K_{111}\omega_0 G_{(111)} a_0 A^{-0.37}}{\pi\sqrt{3}} \frac{\overline{\epsilon^2_{50111}}}{\alpha} \tag{2.3}$$

where $\gamma = stacking\ fault\ energy$

$K_{111}\omega_0 = proportionality\ constant$

$G_{(111)} = shear\ modulus\ in\ the\ (111)\ fault\ plane$

$a_0 = unit\ cell\ edge\ dimension$

$A = Zener\ elastic\ anisotropy$

$\epsilon^2_{50111} = microstrain,\ averaged\ over\ 50\ in\ the\ [111]\ direction$

$\alpha = stacking\ fault\ probability$

There are many quantities in the equation. Some of them are values calculated from the X Ray diffraction experiment while some are material constants which can be taken either from literature or separate experiments/calculations can be done to find them. A complete process chart for calculation of SFE using Eq.[2.3] is shown in Fig.2.7. The section ahead is an elaborate literature review on the experimental determination and literature for these quantities. After Schramm and Reed developed and demonstrated the methodology for X-ray diffraction, researchers adopted the same for neutron diffraction by establishing calculation of the quantities in Eq.[2.3] for neutron diffraction profiles.

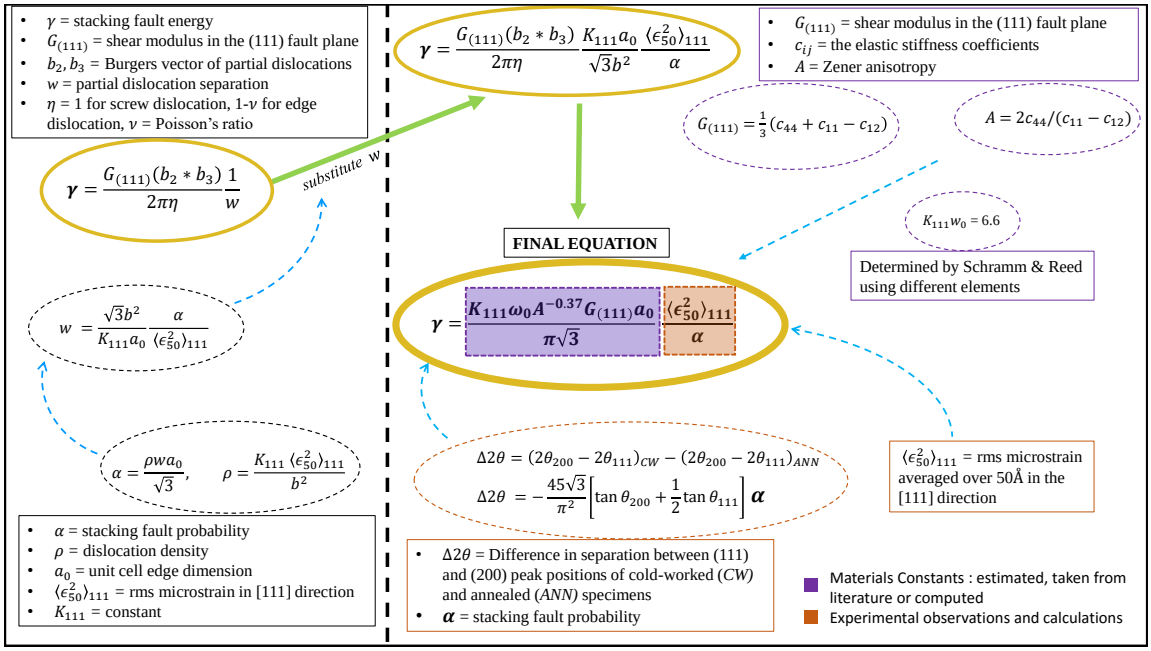

Figure 2.7: Complete procedure for calculation of SFE using X-ray or neutron diffraction in austenitic steels

2.3.2.1 Stacking Fault Probability

Stacking faults occur on the (111) close-packed planes in the fcc crystal and cause shift in position of diffraction lines. Stacking fault probability can be calculated using the angular displacements(shifts) of the of the diffraction peaks according to Warren's method of peak shift analysis.[90]. Comparison between annealed and deformed specimens is typically used to measure the peak shift and get corresponding α. As explained by Reed and Schramm[78], it is best to obtain the profile angular separation of (111) and (200) rather than absolute 2θ positions to avoid diffractometer errors and achieve better sensitivity. Thus the widely used [94, 44, 86, 84, 85, 30, 57, 29] equation to calculate stacking fault probability as given in [78]

$$\begin{aligned} \Delta 2\theta &= (2\theta_{200} - 2\theta_{111})_{CW} - (2\theta_{200} - 2\theta_{111})_{ANN} \\ &= -\frac{45\sqrt{3}}{\pi^2}\left(\tan\theta_{200} + \frac{1}{2}\tan\theta_{111}\right) \end{aligned} \tag{2.4}$$

This equation is derived for (111) and (200) reflections from the general equation described by Warren [90]

$$\Delta 2\theta = \frac{90\sqrt{3}\alpha\tan\theta}{\pi^2 {h_0}^2 (u+b)} \sum_b \pm L_0 \tag{2.5}$$

where $\sum_b \pm L_0/{h_0}^2 (u+b)$ is a constant specific to each hkl reflection. For austenite 111, 200, 220, 311 and 222 reflections, the values are 1/4, -1/2, 1/4, -1/11 and -1/8 respectively[90]. Using the above general form some researchers have calculated α using a different set of reflections[33] or taken averages of α for different set of reflections[46, 45]. To do away with the need of testing a stacking fault free annealed sample for comparison, Talonen et al.[83] described a novel method which combined

Warren's treatment and Baragg's law. By assuming no long range residual stresses in powder sample, the peak positions are affected by lattice spacing and stacking faults which leads to following equation with two unknown parameters (interplanar spacing λ and stacking fault probability α)

$$2\theta_{hkl} = 2arcsin\left(\frac{\lambda}{2d_{hkl}}\right) + \frac{90\sqrt{3}\alpha\tan\theta_{hkl}}{\pi^2 {h_0}^2\,(u+b)}\sum_b \pm L_0 \tag{2.6}$$

Hence Eq.[4] can be used to obtain as many independent linear equations corresponding to each representative hkl austenite reflection. These equations are subsequently solved using linear regression method for α. Talonen et al.[83] and other researchers[5, 54] have described the use of above method for calculation of stacking fault probability in deformed sample eliminating the need of comparison with an annealed sample.

2.3.2.2 RMS Microstrain

X Ray or Neutron Diffraction profile broadening of plastically deformed samples can be caused due to various factors, but primarily due to powder size and strain, hence the profiles can be analyzed for evaluating these 2 components. Various different approaches and software packages exist for the calculation of rms microstrain from the broadening of diffraction profiles. Schramm and Reed[73, 78, 79] in their seminal papers adopted the Warren-Averbach technique [89] in which the value of rms microstrain $\overline{\epsilon^2_{Lhkl}}$ can be expressed as

$$\overline{\epsilon^2_{Lhkl}} = \frac{\left[\ln A_L\left(h_1k_1l_1\right) - \ln A_L\left(h_2k_2l_2\right)\right]a_0^2}{2\pi^2L^2\left[\left(h_2^2+k_2^2+l_2^2\right)-\left(h_1^2+k_1^2+l_1^2\right)\right]} \tag{2.7}$$

where $A_L\left(h_1k_1l_1\right)$ and $A_L\left(h_2k_2l_2\right)$ are the coefficients of the cosine term with first power in the Fourier series expression of diffraction profiles, L a length normal to

reflecting planes, a_0 is the lattice parameter. Typically $(h_1k_1l_1)$ and $(h_2k_2l_2)$ are (111) and (222) planes while as a matter of practice $\overline{\epsilon^2_{L_{hkl}}}$ is averaged over $50\mathring{A}$ in the [111] direction. Instrumental broadening can be eliminated by comparing the profiles for annealed and deformed samples for the same material. In addition to Schramm and Reed many other researchers[94, 84, 85] have used the Warren-Averbach method for calculating rms microstrain. Another widely used [97, 44, 30, 57, 29] method is the Williamson-Hall plot [92] for XRD profiles. Citing probability of errors due to neglecting dislocation density and arrangement effects, some researchers have used a modified Williamson equation along with a modified Warren approach to calculate rms microstrain [5, 54].

3. METHODOLOGY

This work showcases a complete Materials Informatics workflow to solve problems in materials science. There are three integral parts: (i) Data collection and data curation of all experimental calculations of SFE from literature (ii) Using data exploration, visualization to analyze and machine learning algorithms to model the data (iii) Extracting knowledge from the analysis. This chapter will focus on the problem setup, and discuss the first two parts of the informatics workflow methodology.

3.1 Prediction Problem Setup and Uniqueness of Approach

The final objective of this work is to predict SFE for any given Austenitic Steel composition based on just the chemical composition. One approach is to predict the SFE value itself for a given composition. All theoretical physics based computational models essentially do the same, albeit only for limited composition space - upto 4 or 5 different components. Linear Regression techniques applied to SFE data allow for many components, however problems with work in this direction until now have been discussed earlier. Given the high uncertainty in SFE determination, both systemic and experimental, we thought of an approach which would suffice practical needs of SFE determination and be more robust to underlying pattern of data, the composition-SFE relationship.

SFE value is of prime importance in alloy design. Since the SFE value of Austenitic steels drives different deformation mechanisms, for designing a steel with certain grain structure and amenable to required deformation in process-use we need to know the SFE for unknown compositions. However, we certainly do not need the "exact" value or even precise values.

Based on this physical material behavior information, we can construct three

"classes" of SFE or three regimes and can bin all our SFE numerical data to convert it to categorical data. There are two major advantages of this approach: (i) creating classes or regimes helps engulf the systemic and experimental uncertainty associated with experimental SFE calculations. Now we can say that although the SFE calculation may be uncertain numerically with some scatter, it most certainly belongs to a certain regime (ii) the statistical models/machine learning algorithms for modeling such a prediction problem are inherently. We'll discuss more on this in the subsequent sections. As described, once we construct this dataset as a set of compositions and SFE regimes, our prediction problem is essentially a 'classification' task as it is known in machine learning and data mining fields. Given a composition we now want to classify whether the Austenitic Steel belongs to Low or Medium or High SFE regime. This is practically applicable to an alloy design task where compositions can be checked using this classifier and predicted how they would potentially deform which is what SFE is needed for.

3.2 Part I : Data Capture and Curation

A very extensive literature survey has been done to capture all the various experiments done on different Fe alloy systems to build the best possible training dataset for the prediction algorithms. The authors believe that this is the most exhaustive dataset for experimental SFE calculations available to the community yet. The process of data collection was conceived in a manner so that not only the data is captured but also any description that adds information to the data is captured too. Essentially then, metadata regarding the experimental technique, process and conditions which can potentially inform more about the data itself were added too. These data descriptors can help making selections for the training data set, understand patterns on which experimental technique has larger uncertainties etc. and hence

are very useful information.

The process of data collection is the first step but an even important step is data curation. Data curation is the process which essentially enables reliable retrieval and querying of data for future research and reuse. To make our data collection efforts usable and available for the community, we decided to use Materials Data Curation System(MDCS) which is an undertaking by NIST to promote efforts in MGI. Hence we devised a schema for the passing the captured data to a repository in a systematic manner such that the data is query-able as well as re-usable for the community at large. We will release this experimental SFE data for steels repository in MDCS soon after the publication.

3.2.1 Data

We have discussed how SFE is a function of composition and temperature and these are the predictor variables or features which will help in predicting SFE. Though there has been some research on dependence of SFE on grain size, there is very little evidence. Also most experimental research do not report this parameter for the alloys when calculating SFE. Thus we have predominantly captured composition, temperature and SFE. All possible elements that have been used in alloying in austenitic steel system have been considered. We have also discussed various experimental techniques for SFE calculation and underlying reasons on how these calculations can be uncertain. Hence capturing uncertainty in SFE data is crucial and we have reported the spread in SFE values wherever available.

3.2.2 Metadata

In addition to the above mentioned data, descriptors that add meaning and context to the data are equally important. These descriptors might not directly go into the calculations or algorithms for prediction, but are essential for physical relations.

As discussed earlier, there is considerable work in the literature that establishes SFE as a function of processing due to alloying effects. Similarly there is available critique in the literature on the accuracy and applicability of different SFE measurement techniques as well as specific bodies of work. We can take all of these into account to make selections on the complete SFE dataset to choose subsets which we think are the best for a certain problem. However to be able to make these subsets, we need the descriptors of the data - which is essentially the metadata. For the experimental SFE dataset the metadata is broadly bibliography, experimental technique and processing. The bibliography maps observations to particular journal papers which enables us to subset certain observations based on the community's confidence and critique of certain papers. Similarly experimental technique helps choose data only from certain techniques which might be established to be more accurate while processing helps identify differences in SFE measurements based on different process routes.

3.2.3 SFE Dataset

We have a dataset of SFE calculations on various compositions at different temperature conditions processed by different processing routes. This complete dataset has 500 odd points. Table.3.1 is a list of all the papers in the SFE literature from which experimental SFE data was recorded. This to the authors knowledge is the most comprehensive SFE dataset and is exhaustive as far as experimental research in SFE is concerned.

Reference	**Year**	**Technique**
Whelan *et al. [91]*	1959	TEM
Swann *et al. [82],*	1963	TEM
Dulieu *et al.*	1964	TEM
Douglas *et al. [17]*	1964	TEM
Silcock *et al.*	1966	TEM
Clement *et al.*	1967	TEM
Fawley *et al.*	1968	TEM
Thomas *et al.*	1969	TEM
Murr *et al. [60]*	1969	TEM
Latanision *et al. [40]*	1969	TEM
Gallagher *et al. [21]*	1970	TEM
Lecroisey *et al. [43]*	1970	TEM
Latanision *et al. [41]*	1971	TEM
Breedis *et al. [9]*	1971	TEM
Lecroisey *et al. [42]*	1972	TEM
Butakova *et al.*	1973	XRD
Abrassart *et al. [2]*	1973	TEM
Schramm *et al. [78]*	1975	XRD
Volosevich *et al.*	1976	TEM
Strife *et al. [81]*	1977	TEM
Remy *et al. [74]*	1977	TEM
Rhodes *et al. [75]*	1977	XRD
Brofman *et al. [10]*	1978	Literature Survey

Table 3.1: List of all the papers with experimental SFE calculations used to create data repository

Reference	**Year**	**Technique**
Bampton *et al. [4]*	1978	TEM
Stoltz *et al. [80]*	1980	TEM
Yang *et al. [94]*	1982	XRD
Oh *et al. [62]*	1995	TEM
Reick *et al.*	1996	TEM
Pontini *et al. [70]*	1997	TEM
Gavriljuk *et al. [24]*	1998	TEM
Li *et al. [49]*	1999	TEM
Gavriljuk *et al. [23]*	1999	TEM
Kireeva *et al. [38]*	2002	TEM
Petrov *et al. [67]*	2003	TEM
Gavriljuk *et al. [22]*	2006	TEM
Talonen *et al. [83]*	2007	XRD
Bracke*et al. [7]*	2007	TEM
Ojima *et al. [63]*	2009	TEM
Tian *et al. [85]*	2009	XRD
Tian *et al. [85]*	2009	XRD
Li *et al. [50]*	2009	TEM
Lee *et al. [46]*	2010	Neutron Diffraction
Idrissi *et al. [27]*	2010	TEM
Kim *et al. [36]*	2011	TEM
Kim *et al. [35]*	2011	TEM
Kim *et al.*	2011	TEM

Table 3.1 Continued

Reference	**Year**	**Technique**
Mujica *et al.*	2011	TEM
Behjati *et al. [6]*	2011	TEM
Jin *et al. [30]*	2012	XRD
Jeong *et al. [28]*	2012	Neutron Diffraction
Pierce *et al. [68]*	2012	TEM
Unfried-Silgado *et al. [86]*	2012	XRD
Kang *et al. [33]*	2012	Neutron Diffraction
Lee *et al. [45]*	2012	Neutron Diffraction
Yonezawa *et al.*	2013	TEM
Jeong *et al. [29]*	2013	XRD
Pierce *et al. [69]*	2014	TEM
Lehnhoff *et al. [47]*	2014	TEM
Rafaja *et al. [71]*	2014	XRD
Lee *et al. [44]*	2014	XRD
Lee *et al. [44]*	2014	Neutron Diffraction
Lee *et al. [44]*	2014	TEM
Hickel *et al. [25]*	2014	TEM
Barman *et al. [5]*	2014	XRD
Moallemi *et al. [57]*	2015	XRD
Kumar *et al. [39]*	2015	XRD
Mahato *et al. [54]*	2015	XRD
Kim *et al. [37]*	2016	Neutron Diffraction

Table 3.1 Continued

As evident from the table, a large number of papers have been mined to collect this data and build an exhaustive dataset. One merit of this work is the sheer amount of data collected for this task compared to earlier regression approaches in SFE prediction which had data from a maximum of 5 research papers, hence making the data mining task unreliable.

3.3 Part II : Data Analysis and Modeling Techniques

In this section we briefly discuss the Machine Learning(ML) algorithms used in this work on the SFE Dataset. All ML algos work with an input dataset which has observations across various predictors or features. This dataset may or may not have a target value for observations and depending on that an ML algorithm can be classified as supervised or un-supervised. The objective and dataset at hand leads to selection of which ML algorithm one uses with their dataset. Different ML algorithms can be used at different points in a data mining workflow starting from (i) dimensionality reduction which can be useful in working with very high-dimensional data (large number of predictors) and hence capturing only the important ones to reduce dataset size or where dimensionality of data makes it impossible to completely visualize it in three dimensions and hence we reduce dimensions for the purpose of visualization (ii) prediction which depends on our target output type - nominal or categorical. Regression and classification algorithms are used to predict target output based off the predictors/features in the dataset. We use the open source ML Library Sci-Kit Learn [65] in this work.

3.3.1 Dimesionality Reduction and Visualization

The SFE Dataset has 9 predictors - the weight percentage of different alloying elements. We cannot visualize the predictors and SFE value, an 10-dimensional data at once. Hence we have to rely on dimensionality reduction algorithms to reduce

the 10-d data to 2-d or 3-d such that minimal information is lost and we can search for insights after visualizing the data. There can be various approaches to this task and we use 3 different ones to visualize the SFE data. It is important to note that these new dimensions in which we visualize our data might not have any physical meaning or significance but nevertheless help us visualize underlying trends and patterns in the data - if any which would be impossible to visualize in the higher dimensions. The three techniques we use are (i) Principal Component Analysis (ii) Multidimenstional Scaling (iii) Locally Linear Embedding. The common idea in all dimensionality reduction algorithms is based on distance between data points in euclidean space which statistically can be thought of as covariance between points which is tried to be preserved when moving from the high-dimensional mapping to a lower-dimensional representation.

3.3.2 Classification

As explained earlier, our problem definition is prediction of SFE regime or deformation mechanism given a composition of austenitic steel. Hence our target output are classes which are categorical. This problem is essentially a classification task which is a very standard problem in the field of machine learning. It has been discussed in the SFE literature that the compositional dependence in elements space is inherently non-linear. That was one of the main drawbacks of linear regression approaches. Although regression can be used to model non-linear higher order relationships between predictor variables and output class, classification algorithms by virtue of there design are robust to non-linearities and are able to learn faster compared to regression approaches. The three techniques we used are: (i) Random Forests (ii) Support Vector Machines (iii) Artificial Neural Networks The performance of classification algorithms can be measured in different ways, the most common being

using the algorithm on a hold-out test set. The hold-out test set is a subset of the complete data collected which is not used for training or building the model. Hence to the model, it is unseen data. Predicting outputs on inputs from this test set and matching them against actual output is a common way of adjudging performance.

4. RESULTS

Based on the informatics workflow discussed earlier, we delved into the SFE data to look for insights, patterns and then eventually build a classification model. The materials knowledge apriori known to us from literature can be used to support the data analysis, empirical generalization about alloying behavior can be backed by data and vice versa the inconsistencies in the literature can also be pointed otherwise. In the methodology section we explained how we have built a dataset with all experimental SFE data in the literature. The dataset has data for variation of SFE with different alloying additions, however for some alloying elements the data is very less. This makes it impossible to study trends and model SFE for such small sample set of alloying additions.Table 4.1 lists the number of observations in the dataset which have more than 0.05 wt% alloying addition and the highlighted elements have been chosen for the analysis. Additionally only data points for which Fe is the major alloying element have been retained.

Element	**Number of observation**
Ni	**300**
Cr	**332**
Mn	**217**
Mo	**133**
Al	**27**
Si	**120**
C	**98**

Table 4.1: Number of data points in SFE literature for which given alloying element has more than 0.05 wt%

Element	Number of observation
N	**85**
Cu	6
Co	3
Nb	2
Ti	0
V	0
Hf	0
P	7
S	1

Table 4.1 Continued

Also as discussed earlier, the way we are treating the outputs is by considering SFE regimes or classes rather than the numerical values itself. Thus the SFE values were converted to SFE regimes based on the most accepted values in literature : SFE <20 mJ/m^2 = Class 1 or Low, 20 mJ/m^2 <SFE <45 mJ/m^2 = Class2 or Medium and SFE >45 mJ/m^2 = Class 3 or High. A consistent color coding has been followed throughout the results: Low is Blue, Medium is Red and High is Green.

4.1 Data Exploration

Visualizing data leads to many simple yet powerful observations. Just plotting the data along various dimensions and exploring what you see is a very helpful tool in data analysis. There have been many empirical observations and propositions in SFE literature which material scientists use as rules of thumb in alloy design in absence of concrete composition-SFE relationship. These can be useful, however the

generalizations need to be done over a lot of observations. Since we have at our disposal an exhaustive dataset of SFE, we queried and explored the data for visual trends which can be generalized or validate existing ones. We looked at scatterplot matrices where we fixed x-axes as wt % of a particular element and varied other alloying elements on y-axes in different matrices of the scatterplot. Since these are 2-d plots, there is no way to represent SFE numerically with 2 axes taken for wt %. We represent this SFE value dimension by color coding points according to SFE regimes (pointed out in figure labels). Hence while looking at the plots, one should be eying for change in colors in regions which would correspond to certain compositional range leading to a particular SFE regime. We also visualize scatterplots with explicit SFE value vs wt % of certain element to see only the effect of that particular element. Here the color is a redundant value since SFE value is the y-axes, however it helps eyeballing fraction of data in a regime for a particular element.The following is the data exploration analysis with SFE dataset. The salient feature about all the plots is that there really aren't standout patterns and in general the SFE data is very complex with many interplaying factors. Most scatterplot matrices have a mixture of SFE regimes all over the compositions and not much can be said about rules that can explain the data. when looking at scatter plots of SFE value vs wt % alloying element, a given wt % of alloying element exhibits a large range of SFE values practically spanning the whole low-high regime. One can try to look at mean SFE value and look for trends, but that isn't a good approach given this scatter is due to interplay of other elements and averaging will filter that out which beats the purpose. Nevertheless certain elements do show some pattern even with the scatter intact. We look at individual elements next to make specific comments.

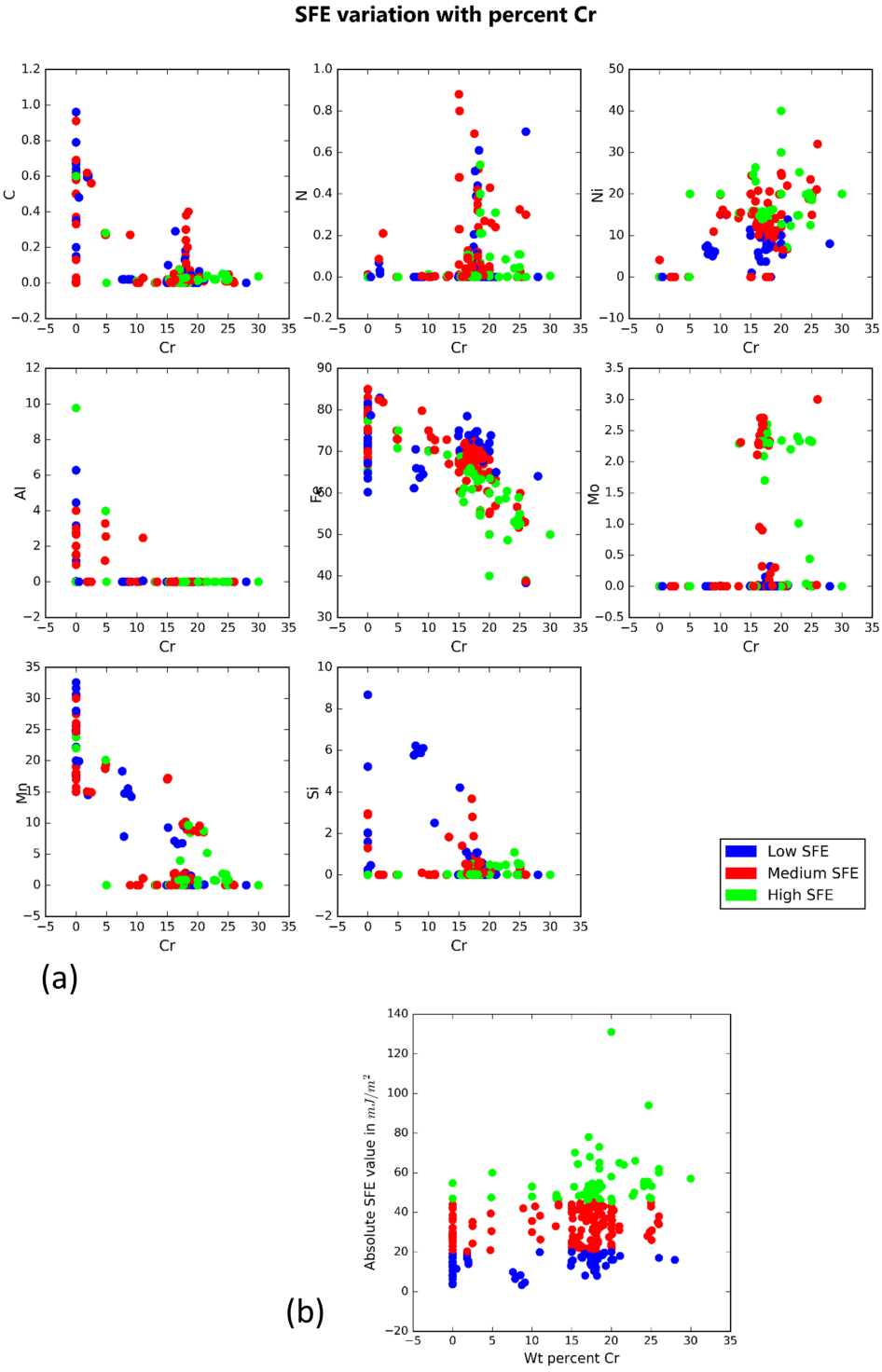

Figure 4.1: (a)SFE data scattermatrix with variation of SFE regimes plotted against weight percent of Cr and other alloying elements (b)Variation of absolute SFE values with weight percent Cr

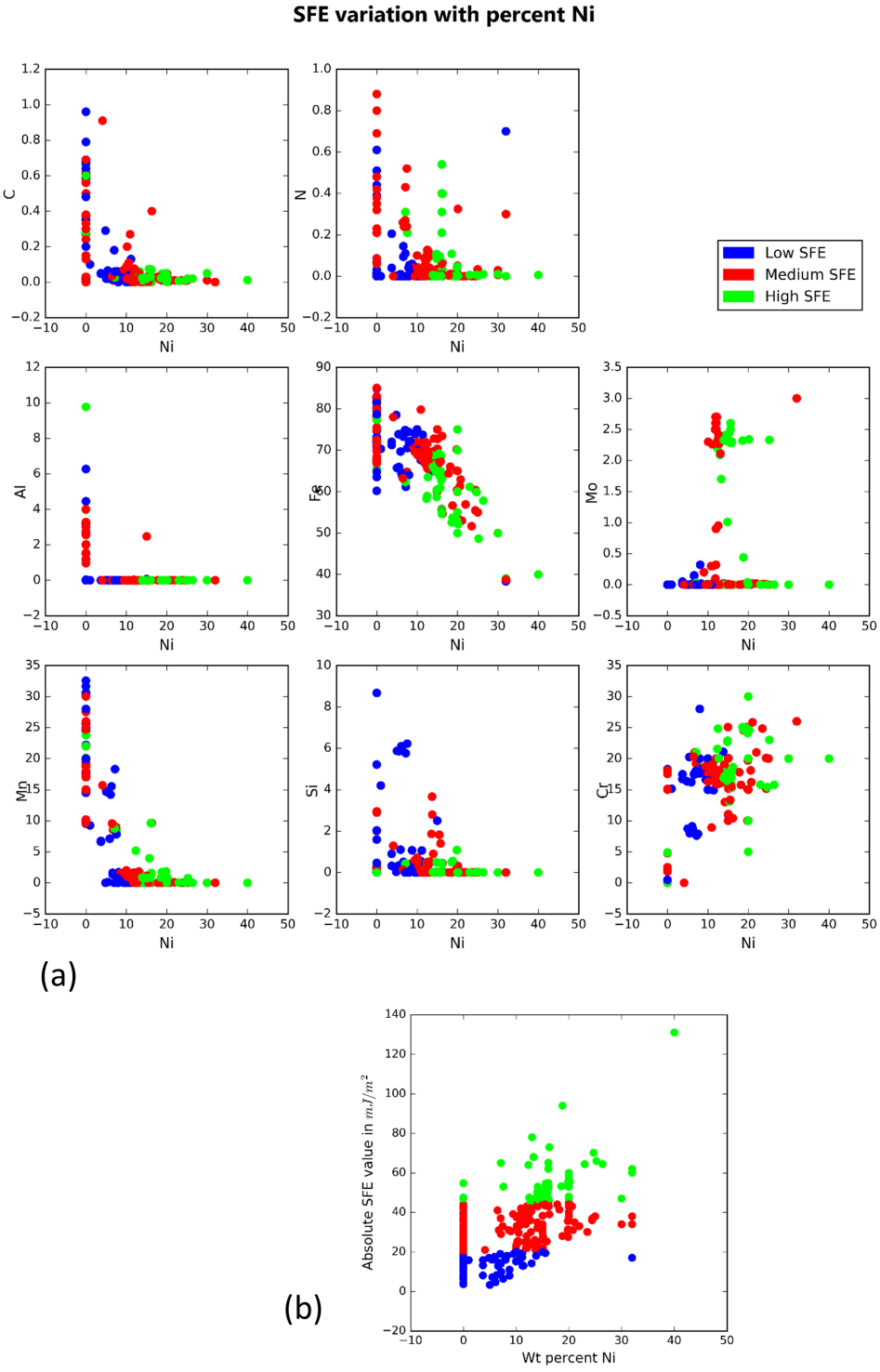

Figure 4.2: (a)SFE data scattermatrix with variation of SFE regimes plotted against weight percent of Ni and other alloying elements (b)Variation of absolute SFE values with weight percent Ni

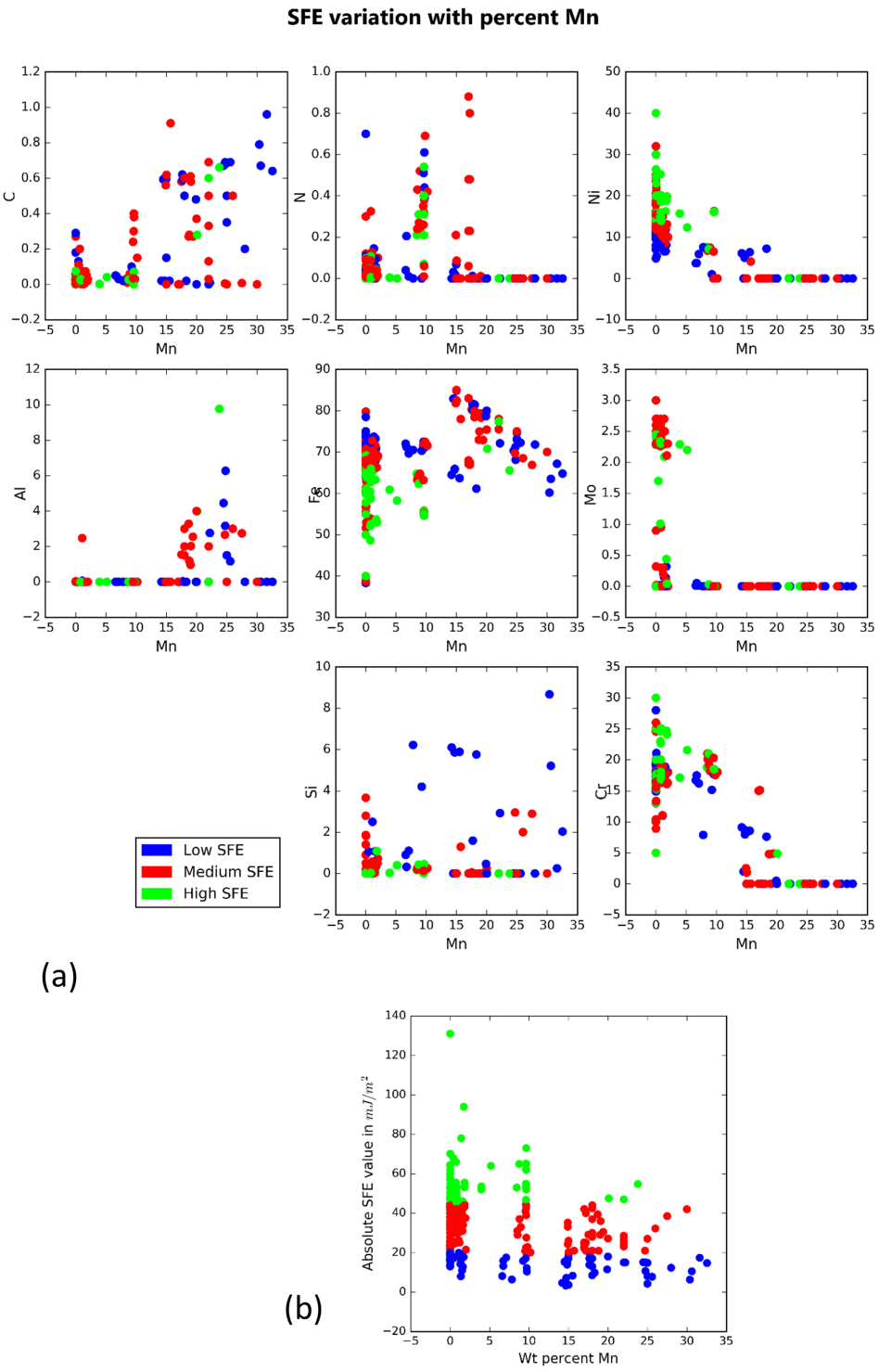

Figure 4.3: (a)SFE data scattermatrix with variation of SFE regimes plotted against weight percent of Mn and other alloying elements (b)Variation of absolute SFE values with weight percent Mn

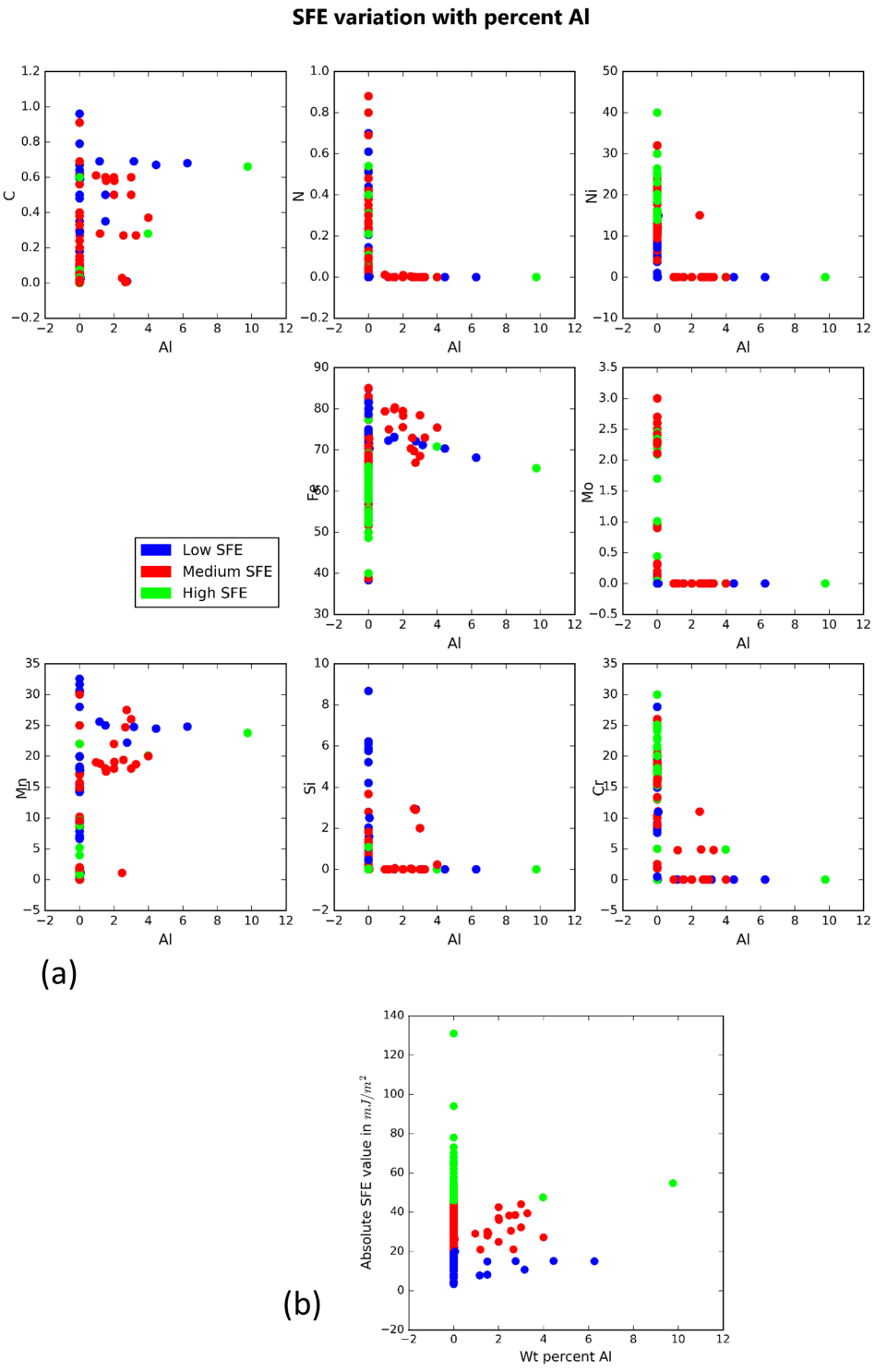

Figure 4.4: (a)SFE data scattermatrix with variation of SFE regimes plotted against weight percent of Al and other alloying elements (b)Variation of absolute SFE values with weight percent Al

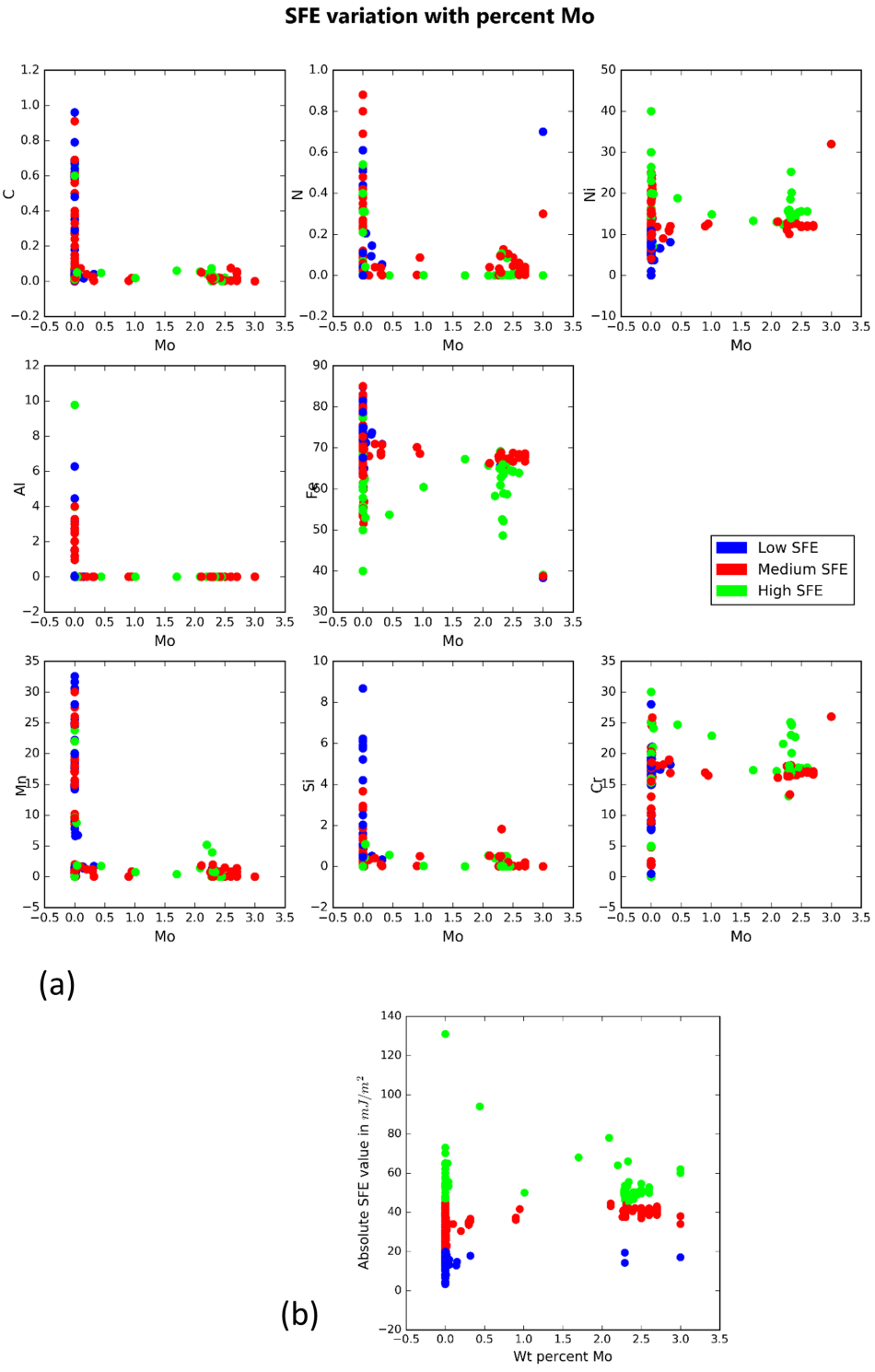

Figure 4.5: (a)SFE data scattermatrix with variation of SFE regimes plotted against weight percent of Mo and other alloying elements (b)Variation of absolute SFE values with weight percent Mo

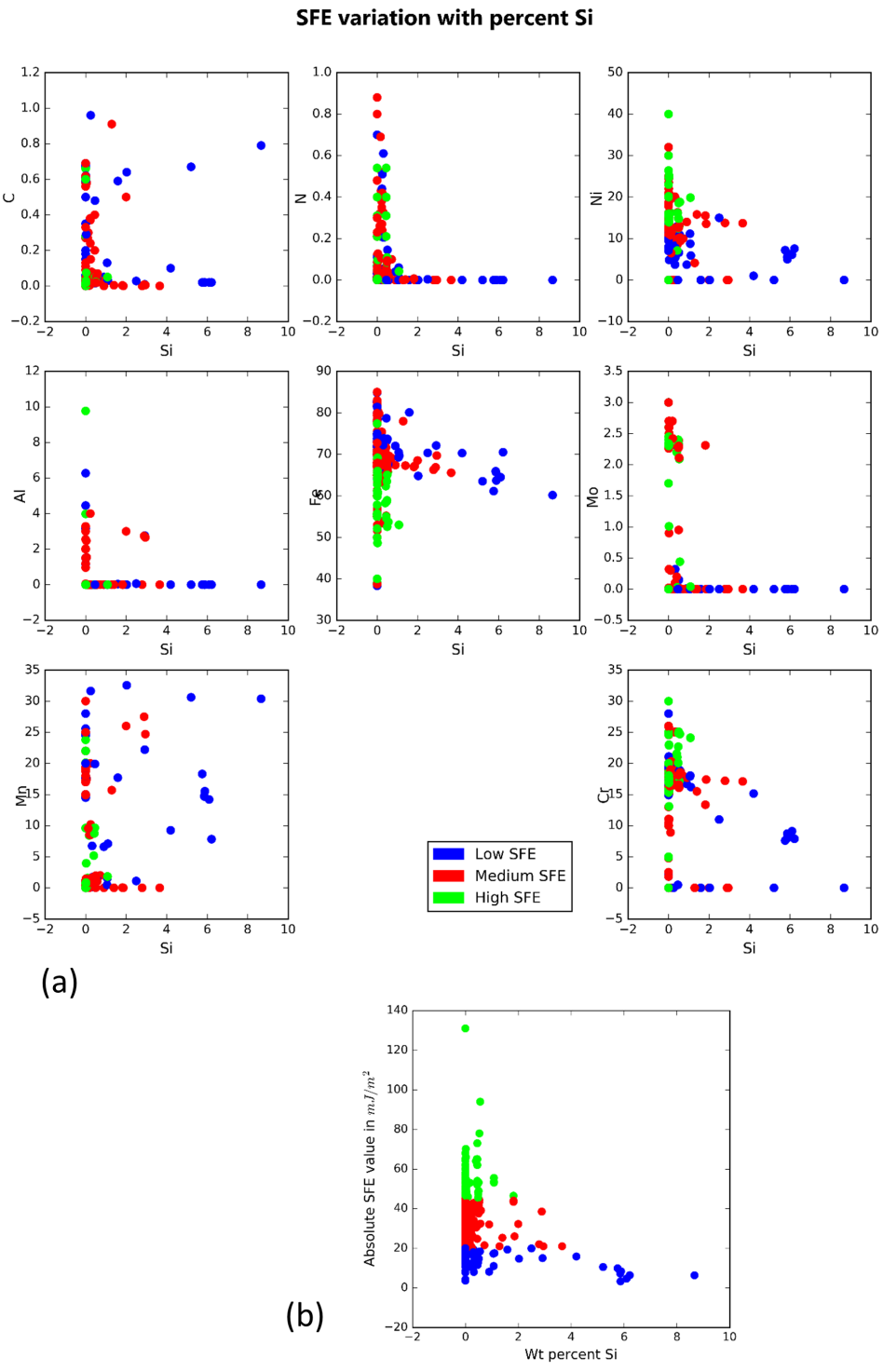

Figure 4.6: (a)SFE data scattermatrix with variation of SFE regimes plotted against weight percent of Si and other alloying elements (b)Variation of absolute SFE values with weight percent Si

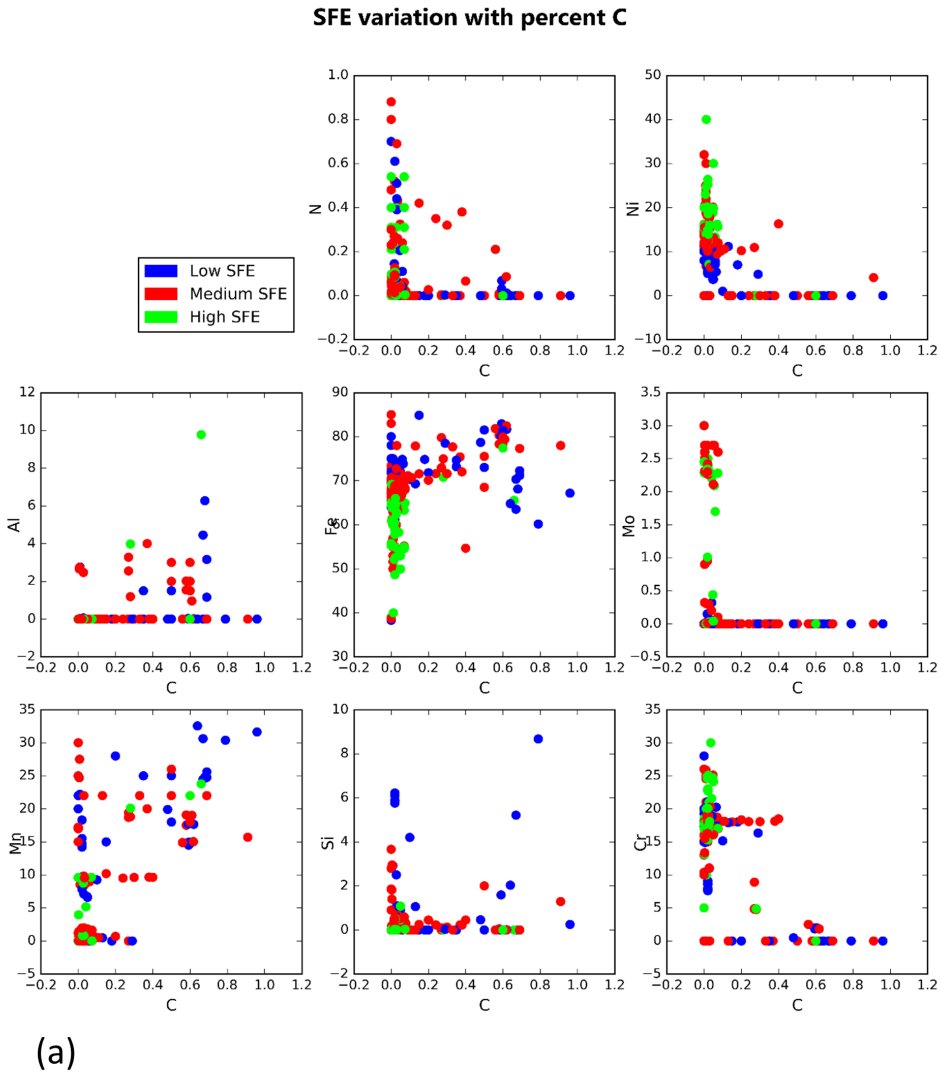

Figure 4.7: (a)SFE data scattermatrix with variation of SFE regimes plotted against weight percent of C and other alloying elements (b)Variation of absolute SFE values with weight percent C

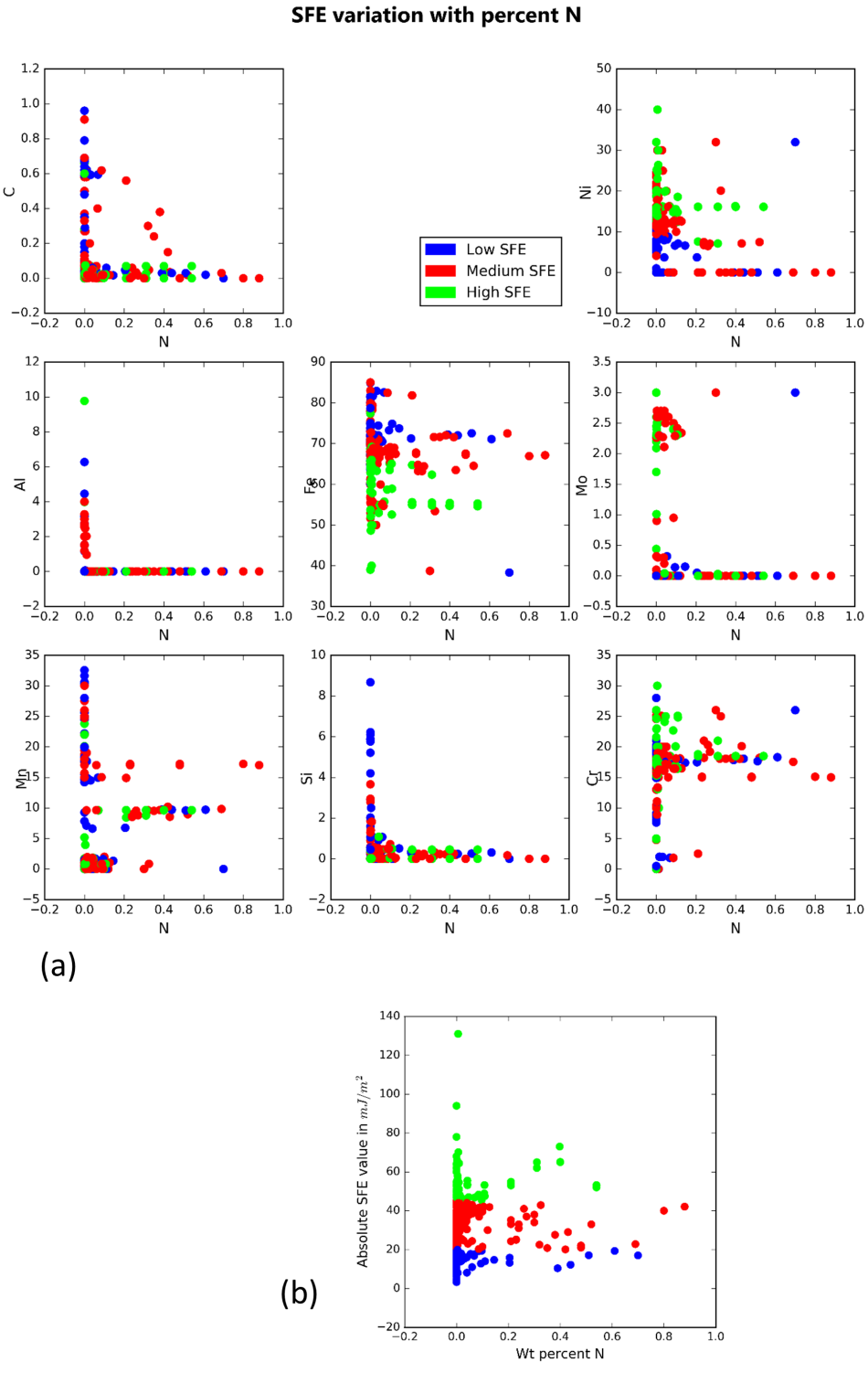

Figure 4.8: (a)SFE data scattermatrix with variation of SFE regimes plotted against weight percent of N and other alloying elements (b)Variation of absolute SFE values with weight percent N

In Fig 4.1 we examine effect of Cr. From Fig 4.1a we can see no outstanding pattern of SFE regime based on interaction of Cr and any other elements. All regimes are mixed and based on wt % of Cr and another element, nothing can be predicted about the possible SFE regime. Examining Fig 4.1b we can see the there is absolutely no relation between SFE and only wt % Cr. For a given Cr alloying, the SFE varies from very low values to very high, thus showing no apparent trend with wt %. Examining Ni, in Fig 4.2a we do see more green points at higher wt % Ni. From Fig 4.2b we see although there is a scatter of SFE values, there is still a clear increasing trend. This is a good validation of the fact in literature that Ni increase SFE. For Mn, from Fig 4.3 again not much can be said about interactions or trends. However it so seems that adding higher amounts of Mn will have very high chances of SFE being in the low and medium regimes as seen by the major absence of high SFE regimes with increasing Mn content except a couple of compositions. In case of Al, the number of observations is very less to make generalizations. From Fig 4.4 we can see there exists no discernible pattern. However in al tested compositions, only 2 observations have led to high SFE regimes in alloys where Al is added. Thus it seems that adding small amounts of Al ($\leq$ 4 wt%) doesn't bump up the SFE too high. Like Cr, looking into Fig 4.5 for Mo does not offer any information. Si is a case where like Ni, a pattern can be deduced. In Fig 4.6b, there is a decreasing SFE trend with increasing Cr even after taking the scatter into account. Fig 4.6a shows more and more low SFE regime towards higher Si content than lower Si contents, thus Si may help reduce SFE if that is the goal. C and N offer not many insights as seen if Figs 4.7 and 4.8.

To summarize, by visual exploration some observations clearly stand out about the SFE dataset that can be related to existing discussion in the literature regarding SFE-composition relationships.

(i) As seen in the plots, the pattern of points going from blue to green (representing increase in SFE) is not monotonic across any dimension and infact highly mixed. Hence this clearly brings out the dependence of composition-SFE relationship of any element on other elements in the system verifying the first-principles calculations regarding non-linear dependencies.

(ii) These plots also clearly thwarts all linear regression equations in the literature listed out earlier as clearly there is no linear relationship between any element and SFE. As emphasized above, there is strong interactions between elements' effects on SFE.

(iii) Not many rules of thumb, generalizations could be processed which might aid in composition tinkering for alloy design. Infact given the non-linearities, it wouldn't be advisable to look for simple rules in composition-SFE relationships.

4.2 Data Visualization

As shown above, visualization can be simple yet powerful technique to look for patterns and know more about the dataset as well underlying relations. However in above data exploration tasks, we were only able to visualize only part of the features of the data at once. Thus we were losing crucial insights about the true nature of SFE dependence on composition. If we could visualize all changing parameters at once and SFE dependence on these parameters, we would essentially know everything. However when the data is higher dimensional than what our viewing permits, complete data visualization becomes increasingly difficult. Here we have to take help of ML algorithms discussed earlier in the thesis. The idea in this section is to compress the 9 dimensional composition space to 2 or 3 dimensions with minimal loss of actual information. We look at the results of three algorithms explained in the methodology.

4.2.1 Principal Component Analysis

As discussed earlier, PCA is a linear dimensionality reduction algorithm. We performed PCA on the SFE dataset and retained the first three components to visualize it in 3 dimensions. Fig 4.9 is the plot of first 3 components of PCA on SFE data.

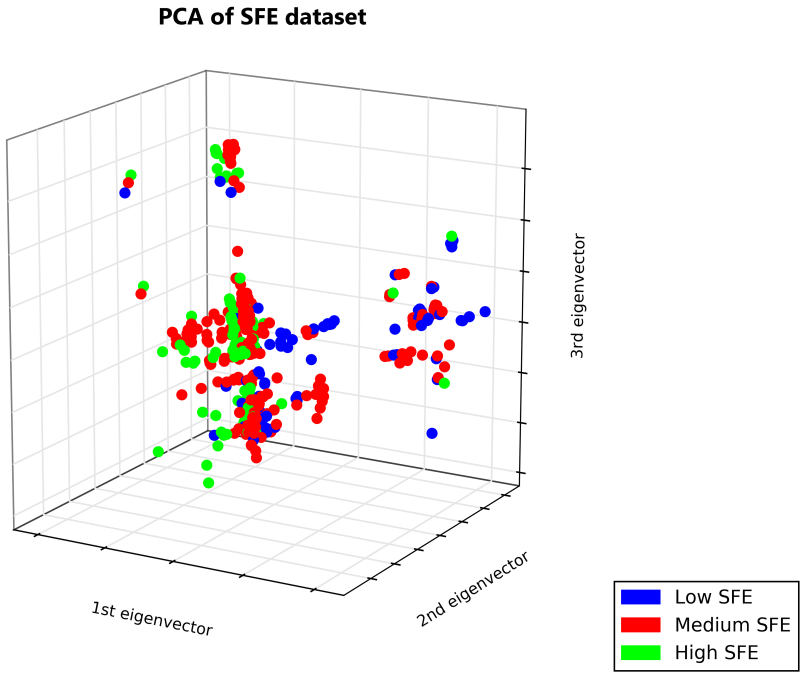

Figure 4.9: Principal component analysis of SFE dataset

The algorithm compresses the 9 dimensional data to 3 dimensional data with 80.5% retention of variance which can be intuitively imagined as the measure of information recovered in this compression. There are no clear regions or clusters of a particular SFE class. To aid in visualization, we take projections of this 3

components to visualize in 2 dimensions. In Fig 4.10 we plot 1^{st} PCA component against the 2^{nd} and 1^{st} against the 3^{rd}. Hence one is the top view and another is the front view of the 3 dimensional plot. Although there still aren't any clear regions corresponding to a specific SFE class. we can use parts of information hidden in these plots to help in our data analysis and modeling.

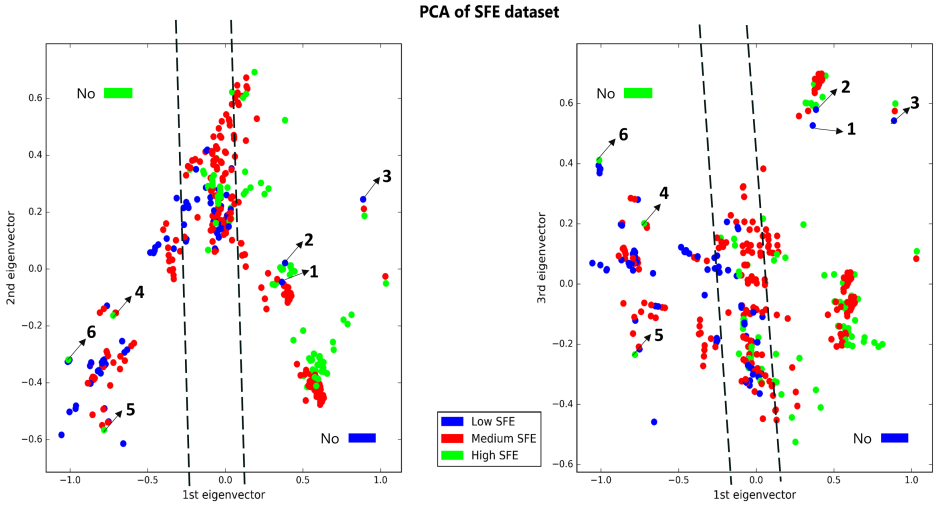

Figure 4.10: Using patterns in PCA to detect unreliable, erroneous and outlier observations

After careful observation we can draw linear boundaries in the projections that has knowledge. For both plots one can see that for PC1 >0.1 approximately, there are almost no observations which fall in low SFE regime. Similarly, for PC <-0.2 approximately, there are almost no observations that fall in high SFE regime. This is a pattern, very simple rules that it in itself can act as a classification rule. If

a new point falls in one one these regions of the plot after transformation, we can say with some certainty what SFE regime it cannot exhibit. However this is not complete information neither the degree of certainty can be quantitatively calculated. Nevertheless we can leverage this pattern to do other analysis of the data. For instance we can look at the very few points which do not follow our proposed pattern and examine the reasoning in the data. Looking for low SFE or blue points in the region PC1 >0.1, we find 3 instances labeled point 1 to 3 in Fig 4.10. Point 1 is a data point from the author Ojima[63]. When we look at compositions very close to this value, we find that there are many observations for SFE regime medium. This is evidence of an unreliable data point in literature to which we can attribute low confidence or choose not to include it while modeling the data. Point 2 is an interesting case. We checked the data for this observation and found out that we had erroneously entered the wrong SFE value while building the dataset from this paper. This point actually corresponds to a point which has an SFE value in the medium regime. Point 3 is an outlier from the general dataset. This has been taken from the author Kireeva[38]. In this paper very small amount of changes in N have been shown to cause very large changes in SFE. Thus this does not fit the proposed pattern, but the accuracy of this calculation cannot be commented on as there are no benchmark observations for comparison. Similarly points which do not follow the other proposed pattern have been labeled from 4 to 6 in Fig 4.10. Point 4 is from the paper by Oh [62]. It's value is on the boundary of changing from medium regime to high regime and since the error is not reported, this pattern is a good reason for considering it in medium regime. Point 5 is from Hickel [25]. This paper studies variation in SFE from processing and temperature. For the same composition, the authors report quite a difference in SFE for very close temperature. And again the SFE value is on the boundary, thus giving a good reason to leverage the pattern and

assign medium regime to this observation. Point 6 is a data observation from author Tian [84]. This is similar to point 3 as the author shows really high jump in SFE value from relatively small increase in Al content. Thus there is a high non-linear effect that PCA cannot accomodate. However in general both proposed patterns follow the data excellently can be used to remove and edit observations as discussed above.

4.2.2 Multidimensional Scaling

Visualizing the SFE dataset after applying multidimensional scaling (MDS) algorithm to reduce dimensions, we can observe the lower dimensional mapping in Fig4.11. The idea was to use a non-linear dimensionality reduction algorithm which potentially might bring out any structure, pattern in the data which can provide information about the composition-SFE relationship. However by looking at Fig4.11 in both dimensions, we see no good pattern or clusters of single SFE regime which can aid in classification.

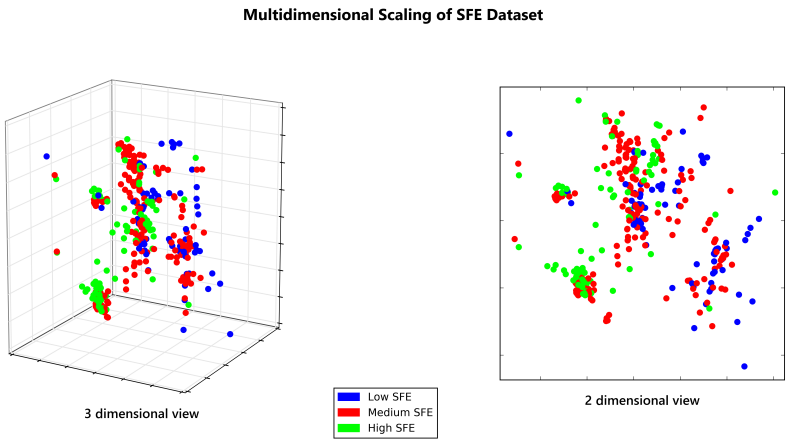

Figure 4.11: Multidimensional Scaling to map SFE data to 3 dimensions(left) and 2 dimensions(right)

Next we try to use this visualization for other analysis as performed with the PCA. Fig4.12 represents the projections of 3 dimensional MDS (Fig4.11), the left plot being the top view and right plot being the front view. Like we did for the PCA projections, here we can draw boundaries in the 2 plots and propose patterns. Quite similar to the PCA patterns, here the region to the right of the boundary is representing space where we should not find low SFE regime compositions and the region to the left of the boundary is representing space where we should not find high SFE regime compositions. When we investigate further outliers to these proposed patterns, we find the exact same data points as in the PCA analysis. Hence our proposed patterns from the data visualizations stand good and can be used as explained in detail in PCA section.

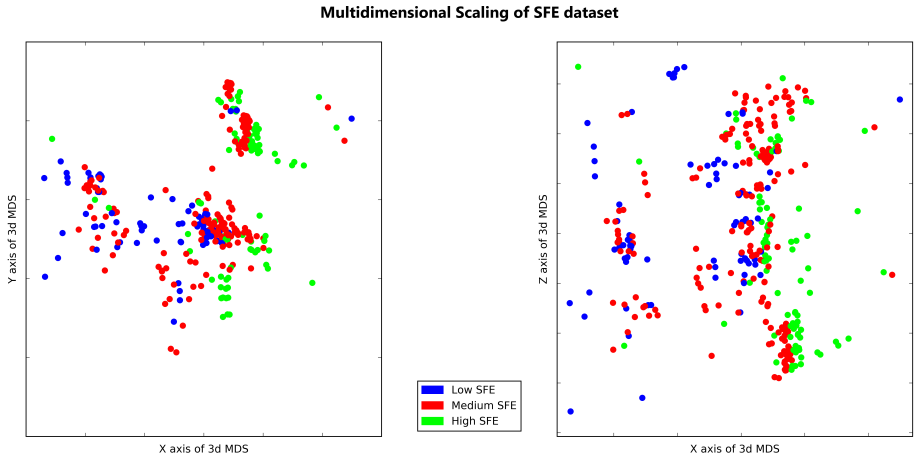

Figure 4.12: Top view (left) and front view (right) of the MDS on SFE data in 3 dimensions

4.2.3 Locally Linear Embedding

We use another nonlinear dimensionality reduction algorithm in the pursuit to find lower dimensional representation which might inform us more about the underlying patterns in the SFE dataset. As mentioned earlier, Locally Linear Embedding algorithm (LLE) tries to search for linear sections in the higher dimensional space and then cuts and pastes those sections in the 2 dimensional space. Fig4.13 shows the application of LLE on SFE dataset. We can observe that in the LLE representation the complete SFE data lies on a shape very close to a V or a Y with a very small vertical base. The most interesting feature of this representation is that each of the arms of this Y has a physical SFE regime correlation. This is precisely what LLE is used for in pattern recognition. As discussed earlier, in a very ideal case different classes separate out on the LLE representation enabling classification from this representation. In the LLE representation of SFE data in Fig4.13 , we can see the left arm (highlighted in yellow) has very less green points or high SFE compositions while the right arm (highlighted in orange) has almost negligible blue points or low SFE compositions. In the earlier 2 visualizations using PCA and MDS we were able to propose similar patterns. However there were no clear boundaries in those representations where we can assert that the pattern exists. LLE helps bring out the pattern explicitly with compositions along the two arms mapped to absence of a particular regime.

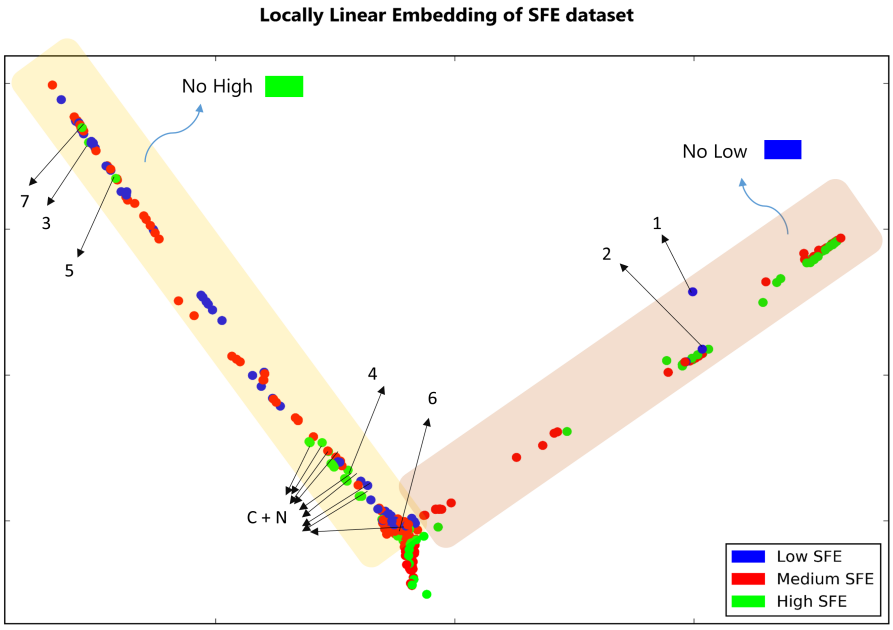

Figure 4.13: Locally Linear Embedding representation of the SFE dataset in two dimensions closely resembling a Y. Left arm highlighted in yellow and right arm highlighted in orange.

Since the classes do not separate out or cluster in regions on the LLE representation, we cannot use this visualization to extract all knowledge about the SFE dependence on composition. However we can again look for exceptions to our proposed pattern visible in the plot to learn more about the data itself. Doing an analysis similar to one discussed above in the PCA section, we find Point 1 and 2 are exceptions to the pattern for the right arm (highlighted in orange). On examining point 1 is the same data point as point 3 discussed in PCA section and point 2 is the same data point as point 1 in PCA section. The reasonings for both these points makes the pattern completely reliable. Now examining exceptions to the pattern on

the left arm (highlighted in yellow), consider points 3, 5 and 7. These are the same as points 6, 4 and 5 from our discussion in PCA section. The reasoning for these exceptions and knowledge gained from them have been explained above. Next we look at the large cluster of points named C+N. All these points are observations from papers by Gavriljuk and Petrov [24, 67, 23, 22]. The common link among them is that these are observations to measure effect of C and N alloying in steels and as discussed earlier as well, the effect of C and N seems to be very significant. According to experiments, small additions lead to large changes. Hence although two compositions can be really close in the LLE embedding due to only a small difference in C or N alloying, they might have very different SFE regimes. Hence all observations measuring effects of interstitials like C and N will most certainly not follow mappings from dimensionality reduction algorithms as is the case here. Looking at remaining exceptions on the left arm, point 4 is an observation from Stoltz [80]. We find that this is an unreliable observation with the calculated SFE quite different from the ones with very similar composition. Given that our proposed pattern seems to be accurate, we can change the regime for this from high to medium SFE. Similarly point 6 is an observation from Schramm [78] and comparing similar compositions, we recommend to change its SFE regime as well.

To summarize, we used various dimensionality reduction algorithms to view the complete SFE data in 2 or 3 dimensions by doing certain transformations. Important learnings from the task are :

(i)We observe the classes are highly mixed in the composition space and there are no regions or cluster for single classes.Had there been any clusters forming or clear boundaries forming, boundaries could have been derived as to what compositions relates to what SFE class. This reinforces the underlying non-linearity and complexity in the data and also draws merit to the use of classification algorithms to link

composition and SFE.

(ii) Nevertheless we could identify 2 patterns in the PCA and MDS representations, regions of absence of compositions with high and low SFE regime. This pattern was identified more concretely with well defined boundary in the LLE representation with the SFE data lying along a Y like shape and each arm corresponding to non-existence of compositions with a certain regime.

(iii) Exceptions to the above proposed pattern were examined. They were either unreliable observations in the literature or outliers. Unreliable observations were recommended to be modified which would help in increasing reliability of data models while outliers were explained as the effects of C and N alloying. Thus this is an excellent showcase of what visual representations can be leveraged for and at the same time their limitations.

4.3 Classification

With the complexity in composition-SFE relationship discussed extensively upto this point, we applied powerful classification algorithms to uncover or "learn" this underlying relationship. Although these classification models are not as intuitively explainable as linear regression which means one cannot write down a final expression relating composition to SFE, it is the price to attain higher accuracy than any existing models. These algorithms can essentially be thus treated as black boxes which when given an input composition, will output the SFE regime or class that the composition belongs to.

The procedure to fit a model to given data was discussed in detail in methodology. We split the SFE dataset randomly into two sets - training set and hold-out test set. We chose a train-test split approach as there has been previous research reported by Braga-Neto and Dougherty [8] which demonstrates that cross-validation method for

estimating performance metrics of classification algorithms can lead to errors in small sample cases. Although the dataset in our case is not as small as what the above paper considers as cases, this method is more robust than cross-validation for small samples. The downside is that we lose some data and hence important information in model training. The proportion decided was 4:1, i.e. 4 parts of data for training set and 1 part for hold-out test set which was split randomly. As mentioned we have applied k-fold cross-validation on our training to train the hyper-parameters of our model and choose the best parameters. The hold-out test set was finally used to compare this best-parametrized models from different algorithms. The comparison metric traditionally used for multi-class classification is accuracy. We report other metrics like precision, recall and false positive rate and then explain why we chose false positive rate as the performance criteria. In addition to this traditional metric we have used another custom metric taking into account the nature of our data and needs of the problem which we discuss later.

The description and results using that is discussed in the next section. Below are the results from the three algorithms we implemented to model SFE data. The golden rule of machine learning, the Occam's razor has been used wherever a parsimonious model had equal or comparable performance to a more complex model.

4.3.1 Support Vector Machines

Support Vector Machines(SVM) are very rich classifiers because of the various types of kernels which can be used to fit the data. The most commonly used kernels which have been proven to give good results are linear, polynomial and radial basis function(rbf) or gaussian. In addition to the kernel, there are two crucial hyperparameters to select in SVMs, C and $gamma$. C is a parameter that acts as a regularizing coefficient balancing misclassifications and simplicity of decision surface.

Hence it is the term which controls overfitting in SVMs. *gamma* is a parameter whose purpose is the same, though it is imagined as the degree of influence of one data point on another. The interplay between these 2 parameters hugely affects SVM performance. For choosing the best parameters and kernel function we did a grid search over combination of parameters and function. The function we chose were the same as listed above and for the parameters we did a logarithmic sweep. K-fold cross-validation accuracy score was the metric for choosing the best parameters. Since the influence of parameters in SVM can vary a lot and the grid has many options, we did cross-validation with large K=30. Since our dataset is small and sparsely sampled in composition space, there can be large variations in training data with a large K. Hence to ensure consistency in training and then compare parameters, we chose such a large K. K-fold cross-validation is known to underestimate accuracy or overestimate errors, but we only use that to choose best parameters. The metric to compare different algorithms is based on the performance of the best-parametrized model on the hold-out or validation set. Fig 4.14 shows the confusion matrix on the validation set from the best SVM model, along with key metrics.

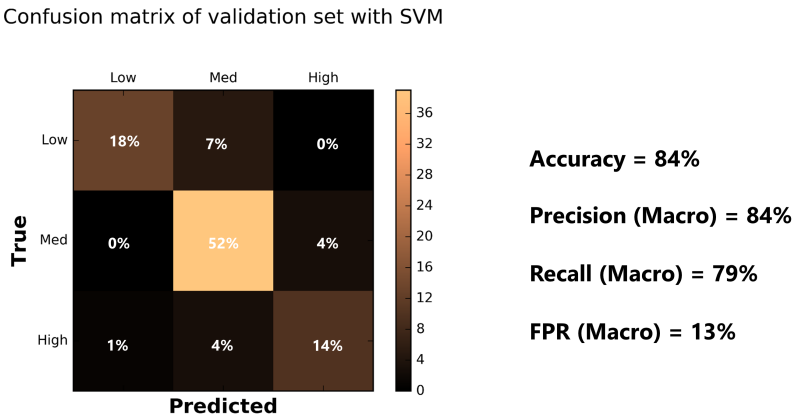

Figure 4.14: Confusion matrix of performance of SVM on validation set

4.3.2 Artifical Neural Networks

Artificial Neural Networks(ANN) are very powerful because of the sheer computational complexity. Given enough parameters, neural networks can learn almost any function irrespective of how non-linear it is. However this can act as a problem since neural networks can easily overfit to the training data leading to poor generalization. Hence sometimes lower models are preferred at the cost of accuracy. ANNs can have many hidden layers and each layer can have many units. The number of layers and units are essentially hyper parameters to the ANN model which decide shape of decision boundary in higher dimension. The activation function in the units of the hidden layer can also be changed but we used a sigmoid function which has been demonstrated to have good performance. There are other parameters like learning rate and number of iterations for searching minima of cost function, but they typically do not affect performance of ANN on unseen data. However they are essential to training performance and minima search. Given the size of our data, we implemented only a 1 hidden layer ANN. The number of units in this hidden layer

and number of iterations were the hyper parameters which we searched for using grid search. Again accuracy score from K-fold cross-validation was used to compare different hyper-parameters. Fig 4.15 shows the confusion matrix on the validation set from the best ANN model, along with key metrics.

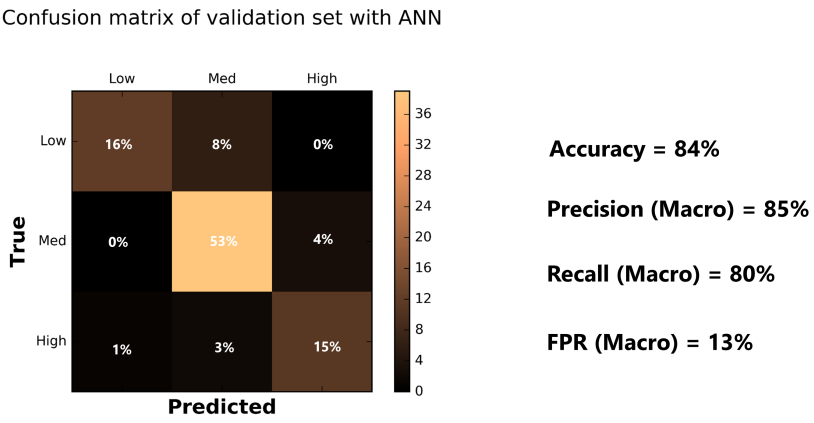

Figure 4.15: Confusion matrix of performance of ANN on validation set

4.3.3 Random Forests

Random Forests (RF) are one of the most popular ensemble machine learning algorithms. They are essentially a collection of many decision trees, but each decision tree in the ensemble is trained differently leading to the 'randomness'. The performance of random forests has been attributed to two key parameters in the literature. First is the number of decision trees used to train the model which leads to many random samples getting selected from the training set since each tree is fit to a bootstrapped sample of the training set. Second is the number of predictors considered at every node to obtain the best split. These 2 hyperparameters essentially control the performance of random forests. We again used K-fold cross-validation

accuracy score as the metric for choosing these hyperparameters. Fig 4.16 shows the confusion matrix on the validation set from the best random forests model, along with key metrics.

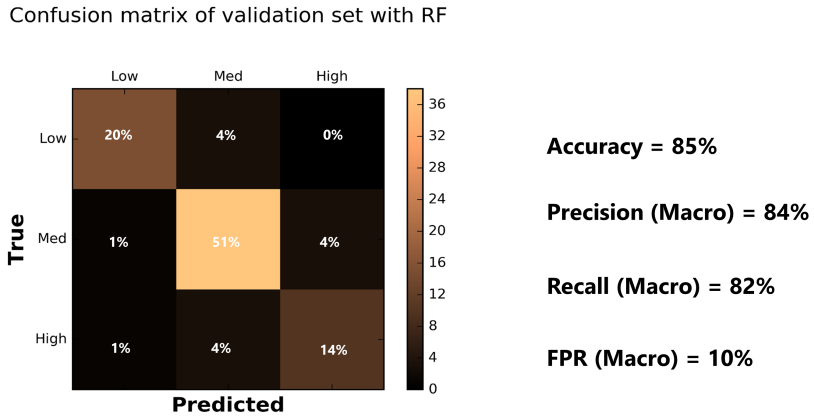

Figure 4.16: Confusion matrix of performance of RF on validation set

4.3.4 Discussion on Performance

As evident from the metrics, all the models have very similar and comparable performance. Each algorithm has an accuracy of about 85% on the validation set. The macro scores of precision and recall are very similar too. We have taken macro scores since all classes are equally important to us and hence no weighting has been provided to better performance over one of the classes. There is a small difference in false positive rate (FPR) which is lower for random forests. This metric is as of now the most important to us as we want this to be as low as possible. Also it has been discussed by Dougherty and coworkers how classification accuracy can vary when the population distributions of the classes are unknown and random sampling cannot be ensured for the training set [20]. Since in this case there is no way to

ensure that all the experimental SFE data collected was randomly sampled, infact there is reason to believe the choice of experiments was dictated by application of alloying systems. Therefore using accuracy as a performance metric is not ideal and we rely on false positive rate which is independent of population distributions and sampling. Thus RF with lowest false positive rate is the model of choice. From the confusion matrices, our learning from data visualization are further emphasized. As can be seen, misclassifications are almost always among Low and Medium or High and Medium classes. There is at maximum 1 misclassification across all models betweem Low and High classes. Thus as evident in the LLE embedding, there is a relatively simple decision boundary separating the Low and High classes. However the boundary between the Medium class and other 2 classes is comparatively fuzzy which can be attributed to lack of data as well as uncertainty in SFE data itself. From the perspective of alloy design and end goal of uncovering composition to deformation regime relationship, we look into another metric to choose make our predictions more reliable and the model more robust.

4.4 Custom Metric for Model Selection

Engineering design is always accompanied by a known factor of safety. Many times better performance is compromised for a more reliable and robust design. With the same principle and philosophy as motivation, we discuss the choice of classification algorithm. We have discussed how this model can be used for alloy design. In alloy design it costlier to make misclassifications then not adding information. For example, if we want to design a steel that exhibits significant twinning and our classifier incorrectly tags a Low SFE composition as Medium in face of just minimal evidence for Low over Medium, it is undesirable. However if the classifier outputs a tag which says that for this composition there isn't enough evidence to assign it to

Low or Medium, we can also check for other compositions. In the process we might lose some candidates, but if we can reduce the incorrect classifications this helps in alloy design.

This evidence is essentially class probability. Most classification algorithms output probabilities of the output being a certain class and then the class with maximum probability is assigned as the output class. This might mean the probabilities being very similar in absolute terms but still having an output class. Though this isn't incorrect, specifically when there is large training data ; in our case with a small dataset and sparse sampling in the composition space coupled with the cost of misclassification, maximum probability isn't robust enough. We need overwhelming evidence of a composition's mapping to a SFE regime. Hence we have to choose a certain threshold probability only above which the model assigns a class, rest of the time it shows that output is fuzzy. Since SVM do not a have a straightforward way of calculating probabilities, we drop them as choice. Between ANN and RF, we chose RF due to its slightly better performance based on false positive rate.

It has been discussed as to how the Low-Medium classes are closely entwined and similarly Medium-High classes. There are two reasons to this. Mathematically due to errors and uncertainty in experimental SFE calculations, for some compositions whose true value lies on the border - there is data with both classes in training set. Another reason is the lack of data as this is relatively a small dataset and hence interpolations are sometimes uncertain. There is a physical materials behavior based reasoning as well. Although there are truly 3 deformation regimes in steels, there is a set of transitioning values between these regimes which has experimental evidence for both regimes. Thus there are two fuzzy zones, one between Low and Medium which we name as Fuzzy-LowMedium and one between Medium and High which we name as Fuzzy-MediumHigh. We do not assign a value to these fuzzy zones as

they are unknown. Mathematically all we can say is that they extend out from the boundaries at 20 mJ/m^2 and 45 mJ/m^2

We decided we want to establish a threshold probability below which our classifier should not assign any class membership. The choice of this probability will be dictated by practical choices between reliability or safety and predictive ability. If we take too stringent a probability we will output a lot of fuzzy choices which is very safe but becomes less predictive as a lot of predictions will lie in the fuzzy zone. If we choose too low, we are basically at the base model. We tried different probabilities greater than 0.5 and below are the results for RF in Table 4.2. The reliability or safety in this case is defined as follows. A prediction is safe if mathematically satisfies the criteria. For instance, a class output of Fuzzy-LowMedium is reliable and safe if the actual SFE is either Low or Medium. One has to realize the reliability is coming from increasing threshold probability which is the gold standard for confidence on an output.

Probability	**Reliability**	**% Fuzzy Outputs**
0.5	86%	3%
0.6	89%	20%
0.66	91%	23%
0.7	93%	35%
0.8	96%	48%

Table 4.2: Metrics for different choice of probabilities to choose output class from RF model

One sees that the safety or reliability is increasing as the threshold probability is increasing but so is the number of fuzzy outputs. The % fuzzy outputs take a huge

jump after 0.5 tp 0.6 which means the base classifier was classifying a lot of points within this range. This is non-ideal as we believe 0.5 isn't high enough a probability for our purposes. However looking for more reliability comes at cost of % fuzzy outputs which if very high, decrease the decision making ability or predictive power of the model. Thus based on above statistics, we choose a threshold probability of 0.66 below which the classifier would tag only fuzzy classes. This is a good enough metric as it ensures the probability of chosen class is almost more than double the probability of any other class. Also at this probability we are classifying about 20% of the inputs fuzzy which we believe as a good price to pay for reliability.

Thus based on our above discussion, now our model outputs 5 classes: Low, Medium, High, Fuzzy-LowMedium and Fuzzy-HighMedium.

4.5 Knowledge Acquisition from Informatics Workflow

In the above sections of the chapter, results at various steps of a Materials Informatics workflow on the SFE dataset have been discussed. The final result of this task was a model which can with good accuracy predict deformation regimes in austenitic steels given composition while safely point out fuzzy zones thereby reducing misclassification. In this section we discuss cases where we used our ML model or insights from the data exploration , hence demonstrating knowledge acquisition from this whole workflow.

4.5.1 Case I : Deformation Regime Prediction

The accuracy of the classification algorithms were adjudged based on the hold-out validation set from the SFE dataset. That is a perfect measure of a model's performance in machine learning. Nevertheless we now wanted to randomly pick some austenitic steel alloys in the literature for which deformation experiments have been carried out and predict their possible deformation behavior from the classifier.

This would be an ultimate litmus test for the model. Table.4.3 is a list of some randomly chosen alloys from literature, their experimentally observed deformation and the model's prediction.

Alloy Composition	**Reference**	**Experimental Observation**	**Model Prediction**
Fe-20.6Mn-0.0Al-0.07Si-0.07C	Sato [77]	ϵ martensite	Low
Fe-19.1Mn-1.8Al-0.14Si-0.07C	-above-	Twinning	Medium
Fe-19.4Mn-4.4Al-0.03Si-0.05C	-above-	Twinning	Medium
Fe-31.3Mn-0.0Al-0.08Si-0.07C	-above-	Twinning	Medium
Fe-29.1Mn-2.0Al-0.11Si-0.07C	-above-	Twinning	Medium
Fe-29.2Mn-3.8Al-0.11Si-0.06C	-above-	Twinning	Medium
Fe-28.8Mn-7.1Al-0.05Si-0.07C	-above-	Twinning	Fuzzy-LowMedium
$Fe_{40}Mn_{40}Co_{10}Cr_{10}$	Deng [14]	Twinning	Fuzzy-LowMedium

Table 4.3: Scoring the ML model against experiments of deformation behavior

As can be seen from the table, the model performs exceptionally well. It was able to predict the correct deformation behavior for most compositions. For the composi-

tions it predicted fuzzy class, the experimental behavior is one of the expected from that fuzzy class. Thus from a design perspective, the fact that the algorithm hasn't misclassified any composition is very crucial. Thus this model can now be used to design alloys with great reliability compared to now when there is no robust model with any defined error bounds. Note for the high entropy alloy the model does not expect any Co input and thus only wt% from other elements were provided.

4.5.2 Case II : Informing Thermodynamic Calculations

We have discussed earlier thermodynamic calculations of SFE based on composition. However the biggest problem in these calculations is ascertaining interfacial energy for which no reasonable estimates are known. Fig 4.17 (left) shows an composition SFE map computed by the Akbari and authors [76]. The colored lines represent SFE = 20 mJ/m^2 for different values of interfacial energy. The interfacial energy is said to be between either of 2 ranges, 5-10 mJ/m^2 and 13-20 mJ^2. An average value of 15 mJ/m^2 has also been suggested. Now based on the choice of this interfacial energy, a given composition on the left of the graph can exhibit SFE from highly negative values to about 20 mJ/m^2. Similarly a point on the right can exhibit SFE values from 20mJ/m^2 to more than 50 mJ/m^2 thus jumping practical SFE regimes. We ran a grid calculation of some compositions from the map and placed their expected regimes on the plot. Here class 1 is Low, class 2 is Medium and class 4 is Fuzzy-LowMedium. As can be seen there is clear evidence of absence of one single interfacial energy value which can describe all these predictions. This reinforces the discussion in their paper where interfacial energy has been shown to be a function of composition. Thus such a composition SFE map needs to be constructed taking into account this dependence. Also the model helps predict practical SFE regimes unlike the large ranges across SFE regimes predicted by the map which makes it unreliable

from a design perspective.

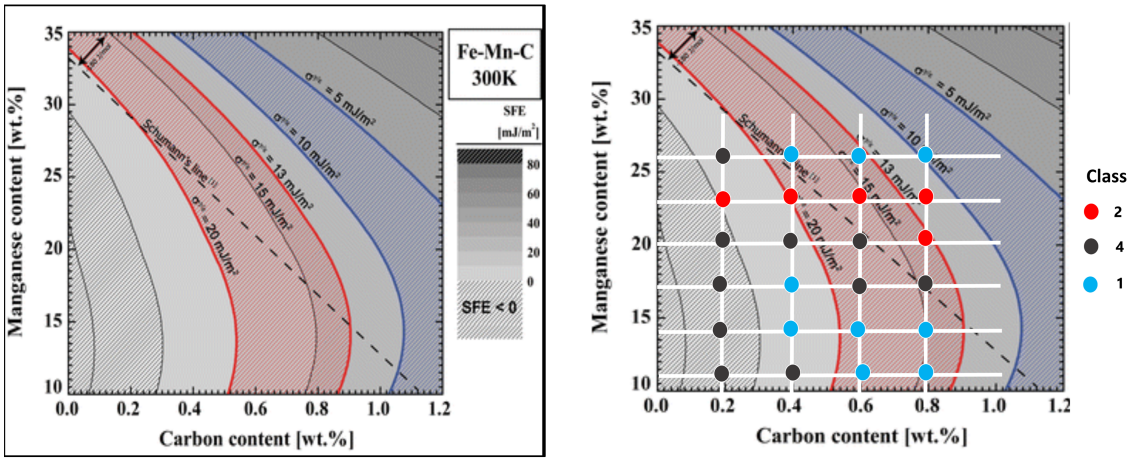

Figure 4.17: Thermodynamic estimation of SFE and ML model predictions

4.5.3 Case III : Experimental Evidence of Computational Trends

As has been shown in the data exploration, we can leverage the exhaustiveness of our experimental dataset to reinforce trends predicted in computational models because more the data, more robust evidence - positive or negative. As discussed earlier, Vitos [87] predicted non-linear relationship between SFE and Ni-Cr alloying in steels. In Fig 4.18, on the left we see DFT predictions of this trend. On the right is all experimental data on Ni and Cr alloying in Fe system and we see good evidence for Vitos' predicted trend. Please note the difference in axis, one is at% and the other is wt%. There is obviously departure from the exact trend as other alloying additions affect SFE. Nevertheless this is another example of how a Materials

Informatics workflow can help the community.

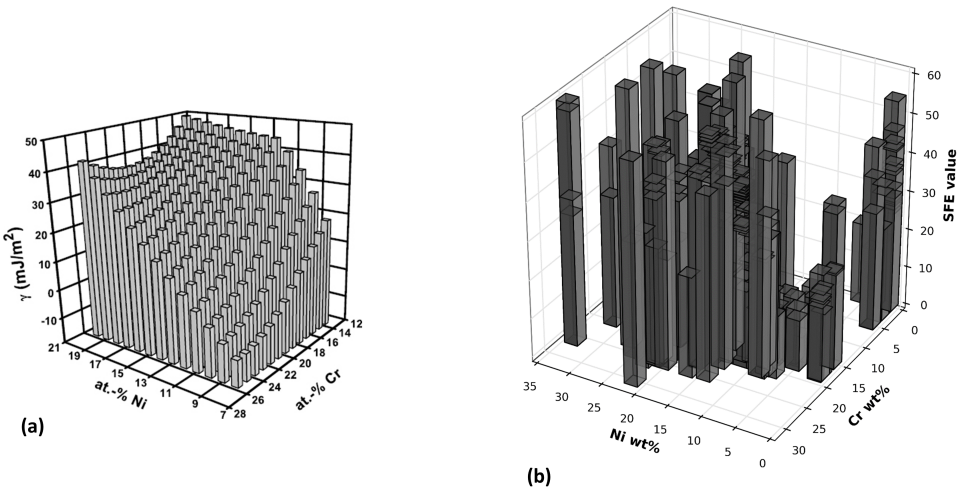

Figure 4.18: (Left)Ni-Cr behavior on SFE from DFT (right) experimental trends in SFE with change in Ni and Cr

5. SUMMARY

In this work we aim to solve the problem of relating composition to SFE in austenitic steels. SFE is crucial to alloy design as it the most important factor which dictates deformation regimes in steels as discussed in the literature. We discuss existing techniques to predict SFE and discuss their pitfalls and lack of reliability. We then propose to use a data driven machine learning approach to model composition SFE relationship based on all experimental data in literature. This approach is first of its kind applied to this particular problem. We setup the problem in a novel way leveraging knowledge about the system. Since a range of SFE values is essential to knowing the deformation regime and not exact SFE values itself, we setup the problem statement as a classification task. We then implemented a complete informatics workflow to solve the problem. As part of this informatics workflow, we first did an exhaustive data curation task collecting and curating all SFE data by reading the literature to form this most exhaustive SFE dataset for austenitic steels known to us. We then applied tools like querying and data exploration to understand simple patters in the data and relate them to literature. Next we applied dimensionality reduction machine learning algorithms to uncover any visualizable patterns. We found patterns in PCA, MDS and LLE representations of the data which separated 2 classes. However the need of applying classification algorithms was clear and we went ahead and modeled data using SVM, ANN and RF. Based on testing with a hold-out test set, we achieved good accuracy of 85% and a good False Positive Rate of 10% with RF . To make our classification prediction more robust, we then do an analysis of choosing a high threshold probability to increase confidence on our predictions. Where the probability output is less than this threshold, we say

the output class is fuzzy. Thus the choice of probability is a balance between having highly confident predictions and having too many fuzzy output classes. We choose a threshold probability of 0.66 which ensures the predicted output class is atleast twice as probable as any other class and this led to 90% safe predictions on our hold-out test set with only 20% of them being classified as fuzzy. Thus we eventually have a machine learning model that predicts Low, Medium or High SFE regimes with high confidence and predicts fuzzy outputs where it is uncertain. Finally we did various tasks to leverage our informatics workflow and showcase its potence. The contribution of this work is that we now have a predictive model that predicts SFE and consequently deformation regimes for untested compositions in austenitic steels with high reliability and good accuracy.

REFERENCES

[1] A. Abbasi, A. Dick, T. Hickel, and J. Neugebauer. First-principles investigation of the effect of carbon on the stacking fault energy of FeC alloys. *Acta Materialia*, 59(8):3041–3048, 2011.

[2] F. Abrassart. Stress-induced $\gamma \rightarrow \alpha$ martensitic transformation in two carbon stainless steels. application to trip steels. *Metallurgical Transactions*, 4(9):2205–2216, 1973.

[3] S. Allain, J. P. Chateau, O. Bouaziz, S. Migot, and N. Guelton. Correlations between the calculated stacking fault energy and the plasticity mechanisms in FeMnC alloys. *Materials Science and Engineering: A*, pages 158–162, 2004.

[4] C. C. Bampton, I. P. Jones, and M. H. Loretto. Stacking fault energy measurements in some austenitic stainless steels. *Acta Metallurgica*, 26(1):39–51, 1978.

[5] H. Barman, A. S. Hamada, T. Sahu, B. Mahato, J. Talonen, S. K. Shee, P. Sahu, D. A. Porter, and L. P. Karjalainen. A stacking fault energy perspective into the uniaxial tensile deformation behavior and microstructure of a Cr-Mn austenitic steel. *Metallurgical and Materials Transactions A*, 45(4):1937–1952, 2014.

[6] P. Behjati and A. Najafizadeh. Role of chemical driving force in martensitic transformations of high-purity Fe-Cr-Ni alloys. *Metallurgical and Materials Transactions A*, 42(12):3752–3760, 2011.

[7] L. Bracke, G. Mertens, and J. Penning. Influence of phase transformations on the mechanical properties of high-strength austenitic Fe-Mn-Cr steel. *Metallurgical and Materials Transactions. Part A*, 37A(2):307–317, 2006.

[8] U. M. Braga-Neto and E. R. Dougherty. Is cross-validation valid for small-sample microarray classification? *Bioinformatics*, 20(3):374–380, 2004.

[9] J. F. Breedis and L. Kaufman. The formation of HCP and BCC phases in austenitic iron alloys. *Metallurgical Transactions*, 2(9):2359–2371, 1971.

[10] P. Brofman and G. Ansell. On the effect of carbon on the stacking fault energy of austenitic stainless steels. *Metallurgical and Materials Transactions A*, 9(6):879–880, 1978.

[11] C. Cheng, R. J. Needs, and V. Heine. Inter-layer interactions and the origin of SiC polytypes. *Journal of Physics C: Solid State Physics*, 21(6):1049, 1988.

[12] S. M. Cotes, A. F. Guillermet, and M. Sade. FCC/HCP martensitic transformation in the Fe-Mn system: Part II. driving force and thermodynamics of the nucleation process. *Metallurgical and Materials Transactions A*, 35(1):83–91, 2001.

[13] S. Curtze and V. T. Kuokkala. Dependence of tensile deformation behavior of TWIP steels on stacking fault energy, temperature and strain rate. *Acta Materialia*, 58(15):5129–5141, 2010.

[14] Y. Deng, C. C. Tasan, K. G. Pradeep, H. Springer, A. Kostka, and D. Raabe. Design of a twinning-induced plasticity high entropy alloy. *Acta Materialia*, 94:124–133, 2015.

[15] P. J. H. Denteneer and W. v. Haeringen. Stacking-fault energies in semiconductors from first-principles calculations. *Journal of Physics C: Solid State Physics*, 20(32):L883, 1987.

[16] A. Dick, T. Hickel, and J. Neugebauer. The effect of disorder on the concentration-dependence of stacking fault energies in Fe1-xMn a first principles study. *Steel Research International*, 80(9):603–608, 2009.

[17] D. L. Douglass, G. Thomas, and W. R. Roser. Ordering, stacking faults and stress corrosion cracking in austenitic alloys. *Corrosion*, 20(1):15t–28t, 1964.

[18] A. Dumay, J. P. Chateau, S. Allain, S. Migot, and O. Bouaziz. Influence of addition elements on the stacking-fault energy and mechanical properties of an austenitic FeMnC steel. *Materials Science and Engineering: A*, 483484:184–187, 2008.

[19] E. El-Danaf, S. R. Kalidindi, and R. D. Doherty. Influence of grain size and stacking-fault energy on deformation twinning in FCC metals. *Metallurgical and Materials Transactions A*, 30(5):1223–1233.

[20] M. S. Esfahani and E. R. Dougherty. Effect of separate sampling on classification accuracy. *Bioinformatics*, page btt662, 2013.

[21] P. C. J. Gallagher. The influence of alloying, temperature, and related effects on the stacking fault energy. *Metallurgical Transactions*, 1(9):2429–2461, 1970.

[22] V. Gavriljuk, Y. Petrov, and B. Shanina. Effect of nitrogen on the electron structure and stacking fault energy in austenitic steels. *Scripta Materialia*, 55(6):537–540, 2006.

[23] V. G. Gavriljuk, H. Berns, C. Escher, N. I. Glavatskaya, A. Sozinov, and Y. N. Petrov. Grain boundary strengthening in austenitic nitrogen steels. *Materials Science and Engineering: A*, 271(12):14–21, 1999.

[24] V. G. Gavriljuk, A. L. Sozinov, J. Foct, J. N. Petrov, and Y. A. Polushkin. Effect of nitrogen on the temperature dependence of the yield strength of austenitic steels. *Acta Materialia*, 46(4):1157–1163, 1998.

[25] T. Hickel, S. Sandlbes, R. K. W. Marceau, A. Dick, I. Bleskov, J. Neugebauer, and D. Raabe. Impact of nanodiffusion on the stacking fault energy in high-strength steels. *Acta Materialia*, 75:147–155, 2014.

[26] J. P. Holdren. Materials genome initiative for global competitiveness. *National Science and Technology Council OSTP. Washington, USA*, 2011.

[27] H. Idrissi, K. Renard, L. Ryelandt, D. Schryvers, and P. J. Jacques. On the mechanism of twin formation in FeMnC TWIP steels. *Acta Materialia*, 58(7):2464–2476, 2010.

[28] J. Jeong, W. Woo, K. Oh, S. Kwon, and Y. Koo. In situ neutron diffraction study of the microstructure and tensile deformation behavior in Al-added high manganese austenitic steels. *Acta Materialia*, 60(5):2290–2299, 2012.

[29] K. Jeong, J.-E. Jin, Y.-S. Jung, S. Kang, and Y.-K. Lee. The effects of Si on the mechanical twinning and strain hardening of Fe-18Mn-0.6C twinning-induced plasticity steel. *Acta Materialia*, 61(9):3399–3410, 2013.

[30] J. E. Jin and Y. K. Lee. Effects of Al on microstructure and tensile properties of C-bearing high Mn TWIP steel. *Acta Materialia*, 60(4):1680–1688, 2012.

[31] J.-H. Jun and C.-S. Choi. Variation of stacking fault energy with austenite grain size and its effect on the Ms temperature of $\gamma \rightarrow \epsilon$ martensitic transformation in FeMn alloy. *Materials Science and Engineering: A*, 257(2):353–356, 1998.

[32] S. R. Kalidindi and M. D. Graef. Materials data science: Current status and future outlook. *Annual Review of Materials Research*, 45:171–193, 2015.

[33] M. Kang, W. Woo, Y.-K. Lee, and B.-S. Seong. Neutron diffraction analysis of stacking fault energy in Fe18Mn2Al0.6C twinning-induced plasticity steels. *Materials Letters*, 76:93–95, 2012.

[34] S. Kibey, J. B. Liu, M. J. Curtis, D. D. Johnson, and H. Sehitoglu. Effect of nitrogen on generalized stacking fault energy and stacking fault widths in high nitrogen steels. *Acta Materialia*, 54(11):2991–3001, 2006.

[35] J. Kim and B. C. D. Cooman. On the stacking fault energy of Fe-18Mn-0.6C-1.5Al twinning-induced plasticity steel. *Metallurgical and Materials Transactions A*, 42(4):932–936, 2011.

[36] J. Kim, S.-J. Lee, and B. C. De Cooman. Effect of Al on the stacking fault energy of Fe18Mn0.6C twinning-induced plasticity. *Scripta Materialia*, 65(4):363–366, 2011.

[37] Y. Kim, Y. M. Kim, J.-Y. Koh, T.-H. Lee, W. C. Woo, and H. N. Han. Evaluation of single crystal elastic constants and stacking fault energy in high-nitrogen duplex stainless steel by in-situ neutron diffraction. *Scripta Materialia*, 119:1–4, 2016.

[38] I. V. Kireeva, Y. I. Chumlyakov, and N. V. Luzginova. Orientation dependence of resolved shear stresses in single crystals of the nitrogen-containing austenitic stainless steel Fe-26% Cr-32% Ni-3% Mo. *Physics of Metals and Metallography*, 93(4):374–383, 2002.

[39] D. Kumar. Design of high manganese steels: Calculation of Sfe and Ms temperature. In *HSLA Steels 2015, Microalloying 2015 & Offshore Engineering Steels 2015*, pages 857–863. John Wiley & Sons, Inc., 2015.

[40] R. M. Latanision and A. W. R. Jr. Extrinsic-intrinsic stacking fault pairs in an Fe-Cr-Ni alloy. *Journal of Applied Physics*, 40(7):2716–2720, 1969.

[41] R. M. Latanision and A. W. Ruff. The temperature dependence of stacking fault energy in Fe-Cr-Ni alloys. *Metallurgical Transactions*, 2(2):505–509, 1971.

[42] F. Lecroisey and A. Pineau. Martensitic transformations induced by plastic deformation in the Fe-Ni-Cr-C system. *Metallurgical Transactions*, 3(2):391–400, 1972.

[43] F. Lecroisey and B. Thomas. On the variation of the intrinsic stacking fault energy with temperature in Fe-18Cr-12Ni alloys. *Physica Status Solidi (A)*, 2(4):K217–K220, 1970.

[44] S.-J. Lee, Y.-S. Jung, S.-I. Baik, Y.-W. Kim, M. Kang, W. Woo, and Y.-K. Lee. The effect of nitrogen on the stacking fault energy in Fe15Mn2Cr0.6CxN twinning-induced plasticity steels. *Scripta Materialia*, 92:23–26, 2014.

[45] T.-H. Lee, H.-Y. Ha, B. Hwang, S.-J. Kim, and E. Shin. Effect of carbon fraction on stacking fault energy of austenitic stainless steels. *Metallurgical and Materials Transactions A*, 43(12):4455–4459, 2012.

[46] T.-H. Lee, E. Shin, C.-S. Oh, H.-Y. Ha, and S.-J. Kim. Correlation between stacking fault energy and deformation microstructure in high-interstitial-alloyed austenitic steels. *Acta Materialia*, 58(8):3173–3186, 2010.

[47] G. Lehnhoff, K. Findley, and B. De Cooman. The influence of silicon and aluminum alloying on the lattice parameter and stacking fault energy of austenitic steel. *Scripta Materialia*, 92:19–22, 2014.

[48] J. Li, M. Zhao, and Q. Jiang. Alloy design of FeMnSiCrNi shape-memory alloys related to stacking-fault energy. *Metallurgical and Materials Transactions A*, 31(3):581–584, 2000.

[49] J. C. Li, W. Zheng, and Q. Jiang. Stacking fault energy of iron-base shape memory alloys. *Materials Letters*, 38(4):275–277, 1999.

[50] X. Li and A. Almazouzi. Deformation and microstructure of neutron irradiated stainless steels with different stacking fault energy. *Journal of Nuclear Materials*, 385(2):329–333, 2009.

[51] K. R. Limmer, J. E. Medvedeva, D. C. V. Aken, and N. I. Medvedeva. Ab initio simulation of alloying effect on stacking fault energy in FCC Fe. *Computational Materials Science*, 99:253–255, 2015.

[52] J. Liu, P. Han, M. Dong, G. Fan, G. Qiao, and J. Yang. Influence of Ni and N on generalized stacking-fault energies in FeCrNi alloy: A first principle study. *Physica B: Condensed Matter*, 407(5):891–895, 2012.

[53] S. Lu, Q.-M. Hu, B. Johansson, and L. Vitos. Stacking fault energies of Mn, Co and Nb alloyed austenitic stainless steels. *Acta Materialia*, 59(14):5728–5734, 2011.

[54] B. Mahato, S. K. Shee, T. Sahu, S. Ghosh Chowdhury, P. Sahu, D. A. Porter, and L. P. Karjalainen. An effective stacking fault energy viewpoint on the formation of extended defects and their contribution to strain hardening in a FeMnSiAl twinning-induced plasticity steel. *Acta Materialia*, 86:69–79, 2015.

[55] N. I. Medvedeva, M. S. Park, D. C. Van Aken, and J. E. Medvedeva. First-principles study of Mn, Al and C distribution and their effect on stacking fault energies in FCC Fe. *Journal of Alloys and Compounds*, 582:475–482, 2014.

[56] A. P. Miodownik. The calculation of stacking fault energies in Fe-Ni-Cr alloys. *Calphad*, 2(3):207–226, 1978.

[57] M. Moallemi, A. Zarei-Hanzaki, and A. Mirzaei. On the stacking fault energy evaluation and deformation mechanism of Sanicro-28 super-austenitic stainless steel. *Journal of Materials Engineering and Performance*, 24(6):2335–2340, 2015.

[58] L. Mosecker and A. Saeed-Akbari. Nitrogen in chromiummanganese stainless steels: a review on the evaluation of stacking fault energy by computational thermodynamics. *Science and Technology of Advanced Materials*, 14(3):033001, 2013.

[59] P. Mullner and P. J. Ferreira. On the energy of terminated stacking faults. *Philosophical Magazine Letters*, 73(6):289–298, 1996.

[60] L. E. Murr. Stacking-fault anomalies and the measurement of stacking-fault free energy in FCC thin films. *Thin Solid Films*, 4(6):389–412, 1969.

[61] J. Nakano. A thermo-mechanical correlation with driving forces for HCP martensite and twin formations in the FeMnC system exhibiting multicomposition sets. *Science and Technology of Advanced Materials*, 14(1):014207, 2013.

[62] B. W. Oh, S. J. Cho, Y. G. Kim, Y. P. Kim, W. S. Kim, and S. H. Hong. Effect of aluminium on deformation mode and mechanical properties of austenitic Fe-Mn-Cr-Al-C alloys. *Materials Science and Engineering: A*, 197(2):147–156, 1995.

[63] M. Ojima, Y. Adachi, Y. Tomota, Y. Katada, Y. Kaneko, K. Kuroda, and H. Saka. Weak beam TEM study on stacking fault energy of high nitrogen steels. *Steel Research International*, 80(7):477–481, 2009.

[64] G. B. Olson and M. Cohen. A general mechanism of martensitic nucleation: Part I. general concepts and the FCC HCP transformation. *Metallurgical Transactions A*, 7(12):1897–1904, 1976.

[65] F. Pedregosa, G. Varoquaux, A. Gramfort, V. Michel, B. Thirion, O. Grisel, M. Blondel, P. Prettenhofer, R. Weiss, V. Dubourg, J. Vanderplas, A. Passos, D. Cournapeau, M. Brucher, M. Perrot, and E. Duchesnay. Scikit-learn: Machine learning in Python. *Journal of Machine Learning Research*, 12:2825–2830, 2011.

[66] X. Peng, D. Zhu, Z. Hu, W. Yi, H. Liu, and M. Wang. Stacking fault energy and tensile deformation behavior of high-carbon twinning-induced plasticity steels: Effect of Cu addition. *Materials and Design*, 45:518–523, 2013.

[67] Y. N. Petrov. Effect of carbon and nitrogen on the stacking fault energy of high-alloyed iron-based austenite. *Zeitschrift fr Metallkunde*, 94(9):1012–1016, 2003.

[68] D. T. Pierce, J. Bentley, J. A. Jimnez, and J. E. Wittig. Stacking fault energy measurements of FeMnAlSi austenitic twinning-induced plasticity steels. *Scripta Materialia*, 66(10):753–756, 2012.

[69] D. T. Pierce, J. A. Jiménez, J. Bentley, D. Raabe, C. Oskay, and J. Wittig. The influence of manganese content on the stacking fault and austenite/ϵ-martensite interfacial energies in Fe-Mn-(Al-Si) steels investigated by experiment and theory. *Acta Materialia*, 68:238–253, 2014.

[70] A. E. Pontini and J. D. Hermida. X-ray diffraction measurement of the stacking fault energy reduction induced by hydrogen in an AISI 304 steel. *Scripta Materialia*, 37(11):1831–1837, 1997.

[71] D. Rafaja, C. Krbetschek, C. Ullrich, and S. Martin. Stacking fault energy in austenitic steels determined by using in situ X-ray diffraction during bending. *Journal of Applied Crystallography*, 47(3):936–947, 2014.

[72] K. Rajan. Materials informatics: The materials "gene" and big data. *Annual Review of Materials Research*, 45:153–169, 2015.

[73] R. Reed and R. Schramm. Relationship between stacking-fault energy and x-ray measurements of stacking-fault probability and microstrain. *Journal of Applied Physics*, 45(11):4705–4711, 1974.

[74] L. Remy. Temperature variation of the intrinsic stacking fault energy of a high manganese austenitic steel. *Acta Metallurgica*, 25:173–179, 1977.

[75] C. G. Rhodes and A. W. Thompson. The composition dependence of stacking fault energy in austenitic stainless steels. *Metallurgical Transactions A*, 8(12):1901–1906, 1977.

[76] A. Saeed-Akbari, J. Imlau, U. Prahl, and W. Bleck. Derivation and variation in composition-dependent stacking fault energy maps based on subregular solution model in high-manganese steels. *Metallurgical and Materials Transactions A*, 40(13):3076–3090, 2009.

[77] K. Sato, M. Ichinose, Y. Hirotsu, and Y. Inoue. Effects of deformation induced phase transformation and twinning on the mechanical properties of austenitic Fe-Mn-Al alloys. *Transactions of the Iron and Steel Institute of Japan*, 29(10):868–877, 1989.

[78] R. Schramm and R. Reed. Stacking fault energies of seven commercial austenitic stainless steels. *Metallurgical Transactions A*, 6(7):1345–1351, 1975.

[79] R. E. Schramm and R. P. Reed. Stacking fault energies of FCC Fe-Ni alloys by X-ray diffraction line profile analysis. *Metallurgical Transactions A*, 7(3):359–363, 1976.

[80] R. E. Stoltz and J. B. V. Sande. The effect of nitrogen on stacking fault energy of Fe-Ni-Cr-Mn steels. *Metallurgical Transactions A*, 11(6):1033–1037, 1980.

[81] J. R. Strife, M. J. Carr, and G. S. Ansell. The effect of austenite prestrain above the Md temperature on the martensitic transformation in Fe-Ni-Cr-C alloys. *Metallurgical Transactions A*, 8(9):1471–1484, 1977.

[82] P. R. Swann. Dislocation substructure vs transgranular stress corrosion susceptibility of single phase alloys. *Corrosion*, 19(3):102t–114t, 1963.

[83] J. Talonen and H. Hnninen. Formation of shear bands and strain-induced martensite during plastic deformation of metastable austenitic stainless steels. *Acta Materialia*, 55(18):6108–6118, 2007.

[84] X. Tian, H. Li, and Y. Zhang. Effect of Al content on stacking fault energy in austenitic Fe-Mn-Al-C alloys. *Journal of Materials Science*, 43(18):6214–6222, 2008.

[85] X. Tian and Y. Zhang. Effect of Si content on the stacking fault energy in γ-Fe-Mn-Si-C alloys: Part i. X-ray diffraction line profile analysis. *Materials Science and Engineering: A*, 516(1):73–77, 2009.

[86] J. Unfried-Silgado, L. Wu, F. Furlan Ferreira, C. Mario Garzn, and A. J. Ramrez. Stacking fault energy measurements in solid solution strengthened Ni-Cr-Fe alloys using synchrotron radiation. *Materials Science and Engineering: A*, 558:70–75, 2012.

[87] L. Vitos, P. A. Korzhavyi, J.-O. Nilsson, and B. Johansson. Stacking fault energy and magnetism in austenitic stainless steels. *Physica Scripta*, 77(6):065703, 2008.

[88] L. Vitos, J. O. Nilsson, and B. Johansson. Alloying effects on the stacking fault energy in austenitic stainless steels from first-principles theory. *Acta Materialia*, 54(14):3821–3826, 2006.

[89] B. Warren and B. Averbach. The effect of cold-work distortion on X-ray patterns. *Journal of Applied Physics*, 21(6):595–599, 1950.

[90] B. E. Warren. *X-ray Diffraction*. Courier Corporation, 1969.

[91] M. J. Whelan. Dislocation interactions in face-centred cubic metals, with particular reference to stainless steel. *Proceedings of the Royal Society of London A: Mathematical, Physical and Engineering Sciences*, 249(1256):114–137, 1959.

[92] G. Williamson and W. Hall. X-ray line broadening from filed aluminium and wolfram. *Acta Metallurgica*, 1(1):22–31, 1953.

[93] R. Xiong, H. Peng, H. Si, W. Zhang, and Y. Wen. Thermodynamic calculation of stacking fault energy of the FeMnSiC high manganese steels. *Materials Science and Engineering: A*, 598:376–386, 2014.

[94] S. Yang and J. Spruiell. Cold-worked state and annealing behaviour of austenitic stainless steel. *Journal of Materials Science*, 17(3):677–690, 1982.

[95] W. S. Yang and C. M. Wan. The influence of aluminium content to the stacking fault energy in Fe-Mn-Al-C alloy system. *Journal of Materials Science*, 25(3):1821–1823, 1990.

[96] T. Yonezawa, K. Suzuki, S. Ooki, and A. Hashimoto. The effect of chemical composition and heat treatment conditions on stacking fault energy for Fe-Cr-Ni austenitic stainless steel. *Metallurgical and Materials Transactions A*, 44(13):5884–5896, 2013.

[97] A. Zaddach, C. Niu, C. C. Koch, and D. L. Irving. Mechanical properties and stacking fault energies of NiFeCrCoMn high-entropy alloy. *JOM*, 65(12):1780–1789, 2013.